

LINEAR QUADRUPOLE FOCUSING FOR HIGH RESOLUTION MICRODROPLET-
BASED FABRICATION

by

Stephen F Heston

BS, University of Pittsburgh, 2002

Submitted to the Graduate Faculty of

the School of Engineering in partial fulfillment

of the requirements for the degree of

Master of Science

University of Pittsburgh

2004

UNIVERSITY OF PITTSBURGH

SCHOOL OF ENGINEERING

This thesis was presented

by

Stephen F Heston

It was defended on

November 29, 2004

and approved by

Michael Lovell, Associate Professor, Department of Industrial Engineering

Marlin Mickle, Professor, Department of Electrical Engineering

Laura Schaefer, Assistant Professor, Department of Mechanical Engineering

Thesis Advisor: Michael Lovell, Associate Professor, Department of Industrial Engineering

LINEAR QUADRUPOLE FOCUSING FOR HIGH RESOLUTION MICRODROPLET-BASED FABRICATION

Stephen F Heston, MS

University of Pittsburgh, 2004

In industry, particularly in the field of rapid prototyping, droplet-based manufacturing is proving to be an extremely efficient technique for the production of low cost electronic components. However, for some applications, the desired material properties at deposition are not easily integrated with a homogeneous, low viscosity fluid suitable for droplet ejection. For this reason, it would prove beneficial to have some means of altering the material properties of the droplets during their travel to the substrate. Due to the inherent irregularities in droplet ejection systems, increases in the associated throw-distances and travel times generally cause decreased resolution in placement. Thus, the purpose of this study was to assess the potential of a linear electrodynamic quadrupole for use in constraining the trajectories of charged microdroplets to allow for modification of their material properties prior to deposition. The equations of motion for the droplets within the device were derived and integrated numerically. Approximate bounds on the system stability were determined and the effects of the respective parameters were considered. An experimental system was constructed and used for deposition experiments. The results obtained, show that a linear quadrupole can be used to focus microdroplet streams for deposition, and that the corresponding operating variables can be predicted from the governing equations.

TABLE OF CONTENTS

1.0 INTRODUCTION	1
1.1 INKJET PRINTING	1
1.1.1 Continuous Inkjet	2
1.1.2 Drop-On-Demand	4
1.2 QUADRUPOLE FOCUSING	5
2.0 THEORY	9
2.1 DROPLET CHARGING	9
2.1.1 Fluid Jet Polarization	9
2.1.2 Rayleigh Instability	10
2.1.3 Electrostatic Deflection	10
2.2 FLUID FLOW	11
2.3 QUADRUPOLE FOCUSING	13
2.3.1 The Quadrupole Field	13
2.3.2 Equations of Motion	15
2.3.3 Stability	16
3.0 NUMERICAL CALCULATIONS	19
3.1. PARTICLE TRAJECTORIES	19
3.2. DROPLET EVAPORATION	28
3.3. VERTICAL MOTION	31

4.0 EQUIPMENT AND SETUP	33
4.1 DROPLET EJECTION	33
4.2 FLUID PROPERTIES	34
4.3 SUBSTRATE AND POSITIONING	35
4.4 CHARGING MECHANISM	36
4.5 DEFLECTION	37
4.6 IMAGING SYSTEM	38
4.7 THE QUADRUPOLE DEVICE	40
5.0 EXPERIMENTS AND RESULTS	43
5.1 DROPLET EJECTION	43
5.2 CHARGING AND DEFLECTION	46
5.3 QUADRUPOLE FOCUSING	48
5.4 DEPOSITION	55
6.0 SUMMARY AND CONCLUSIONS	58
BIBLIOGRAPHY	61

LIST OF TABLES

Table 1: Properties of the commercial and experimental inks.....	35
--	----

LIST OF FIGURES

Figure 1.1: Schematic of a Continuous-Ink-Jet Printer.....	3
Figure 1.2: Several forms of drop-on-demand ejectors.....	4
Figure 1.3: Effect of Fluid Properties on Feature Geometry.....	6
Figure 1.4: Geometry of a linear quadrupole with hyperbolic electrodes.....	7
Figure 2.1.1: Droplet Charging with Fluid Jet Polarization.....	9
Figure 2.3.1: Equipotential curves of a quadrupole field.....	14
Figure 2.3.2: Schematic of a Linear Quadrupole Mass Filter.....	16
Figure 2.3.3: The lower stability region usually used in mass filter operation.....	17
Figure 3.1.1: Particle trajectory in x-direction for: $\omega = 400$, $a = 40\mu\text{m}$, $r_0 = 1.38\text{mm}$	20
Figure 3.1.2: Particle trajectories for several values of q	21
Figure 3.1.3: Restoring rate in terms of the number of oscillations of the field.....	22
Figure 3.1.4: Maximum displacement experienced by a particle for different values of the parameter q	24
Figure 3.1.5: Maximum displacement of a particle for several initial velocities.....	25
Figure 3.1.6: Maximum Displacements for several different initial velocities and an initial phase of $\phi = \pi / 2$	26
Figure 3.1.7: Focusing time for several initial conditions.....	27
Figure 3.2.1: Trajectory and changing value of q for an evaporating droplet.....	29
Figure 3.2.2: Divergence of an evaporating droplet from the quadrupole.....	30
Figure 3.2.3: Oscillation amplitudes for a diverging trajectory.....	31

Figure 3.3.1: Plot of vertical position for an evaporating droplet.....	32
Figure 4.1.1: Image and schematic of the piezoelectric drop generator.....	33
Figure 4.3.1: Aerotech 2-dimensional xy-stage.....	36
Figure 4.4.1: Image of the droplet charging mechanism.....	37
Figure 4.5.1: Image and schematic of droplet charging and measurement setup.....	38
Figure 4.6.1: Image of the CCD camera and mounting system.....	39
Figure 4.7.1: Image of the linear quadrupole device.....	41
Figure 4.7.2: An image of the testing system for quadrupole focusing experiments.....	42
Figure 4.7.3: Signals and Controls for quadrupole focusing experiments.....	42
Figure 5.1.1: Images of (1) unstable ejection, (2) satellites, (3) single droplet.....	44
Figure 5.1.2: Images of velocity progression for ejected microdrops.....	45
Figure 5.1.3: Plot of experimental and numerical data.....	46
Figure 5.2.1: Images of droplet motion in a uniform electric field.....	47
Figure 5.2.2: A plot of the calculated droplet charge according to the voltage applied to the charge tunnel electrodes.....	48
Figure 5.3.1: Geometry of the quadrupole entrance region.....	49
Figure 5.3.2: Numerical simulation of droplet trajectories.....	50
Figure 5.3.3: Images of droplets (1) entering the device (2) 60mm downstream.....	51
Figure 5.3.4: Images of (1) focused droplets (2) unstable trajectories.....	53
Figure 5.3.5: Numerical results of maximum displacements for experimental conditions.....	54
Figure 5.4.1: Marks created with standard DOD and with quadrupole focusing.....	56

1.0 INTRODUCTION

1.1 INKJET PRINTING

Inkjet printing is well established as a versatile and efficient method for applying text and graphics to various substrates. In industry it has revolutionized product identification with the ability to adjust marks dynamically on the production line. In the past several decades, the applications of this technique have broadened from simple visual graphics to a general method for material deposition. It has proven invaluable in areas ranging from drug delivery in the biological sciences to the production of low-cost electronic components using additive fabrication. It is this latter area with which the present paper is concerned.

Droplet-based manufacturing (DBM) is a production method that utilizes inkjet printing to deposit small quantities of fluid. This fluid contains a dissolved or suspended substance, which, upon curing, forms the resulting physical feature. The placement of the material is controlled primarily with the positioning of the substrate. The deposition and substrate motion are synchronized so that adjacent drops overlap and join to form a continuous trace. In this way, two-dimensional and some simple three-dimensional features can be produced.

As with traditional inkjet printing, the primary benefit of this technique is its versatility during production. The design of the feature to be printed may be altered from one print to the next with only simple changes in the electronic controls to the system. It eliminates the need for retooling and minimizes the changeover time between parts. Also, this method is extremely efficient from a material standpoint. Because it is an additive process, it generates no waste, except for the products of decomposition, which depend entirely on the application. For these

reasons, DBM has proven extremely useful in the field of rapid prototyping, where sequential parts are rarely identical, and short changeover times are important.

Two major forms of inkjet printing are commonly used in industry for material deposition. These are continuous-ink-jet (CIJ) and drop-on-demand (DOD).

1.1.1 Continuous-Inkjet

CIJ is a technique used primarily in product identification where high print rates and relatively small characters are desired. This method relies on the charging and electrostatic deflection of droplets for their placement on the substrate. In a CIJ print head, the fluid is forced out of a nozzle by positive pressure as a continuous stream. Inside the nozzle, a piezoelectric element (PZT) modulates at a certain constant frequency, creating a periodic pressure wave in the exiting fluid column. This wave causes the fluid stream to break up into droplets of equal size at the same frequency as the PZT modulation. The internal system pressure, along with the nature of the PZT motion, defines the velocity and size of the droplets. In order to control the amount of electric charge residing on the drops, a charging electrode, or 'charge tunnel,' is placed at the point of droplet breakup. By the application of a voltage potential across this electrode and the print head nozzle, a charge gradient is induced in the fluid stream and the droplets break off with an imbalance of electric charge. After a droplet passes the charge tunnel, it continues through two parallel capacitor plates. A large DC voltage is applied across these deflector plates, creating an electric field normal to the droplet velocity. A droplet void of electric charge travels unaffected through this field and is caught by a recirculation gutter, which returns the ink to the system reservoir. However, a charged droplet will be deflected as it traverses this field by an amount proportional to the magnitude of its contained charge. A schematic of a CIJ print head is shown in Figure 1.1, of page 3.

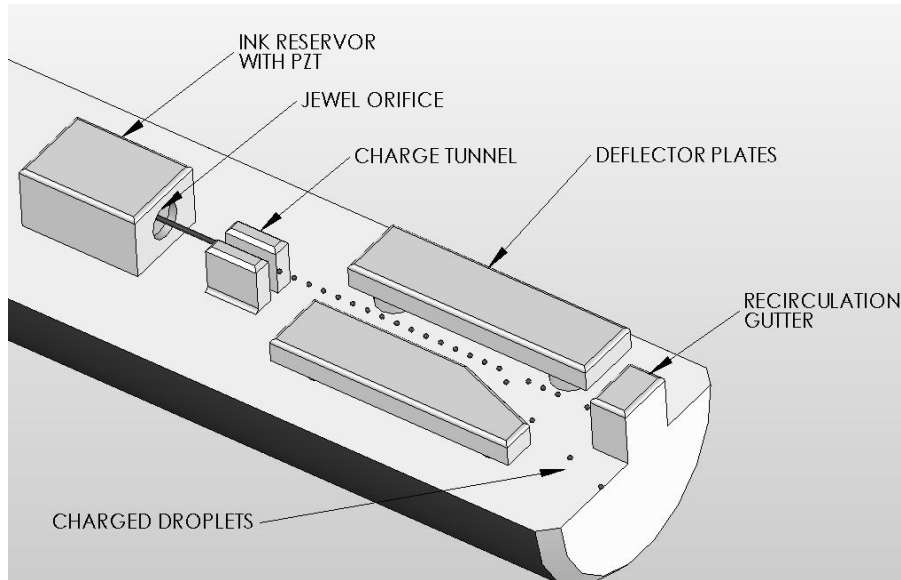


Figure 1.1: Schematic of a Continuous-Ink-Jet Printer.

So, by adjusting the voltage applied to the charge tunnel at the instant of droplet breakup, the amount of charge on a droplet and thus its placement on the substrate can be controlled. The high velocities and fast generation rates of droplets ejected with CIJ printers allow for long throw distances and high speed deposition. Also, because this type of system uses a large internal pressure to create a constant, fast moving stream of fluid, it is possible to eject inks of relatively high density and viscosity. The continuous circulation of the fluid reduces the coagulation of particles and helps to maintain homogeneity in suspensions.

One shortcoming of this technique is the need for the ejected fluid to have a high electrical conductivity. In order to charge the droplets, the fluid must allow for the transport of electrons through the exiting column. Generally, ionic components are added to the ink formulation to achieve the desired electrical properties.

1.1.2 Drop-On-Demand

DOD is the most commonly used form of inkjet printing. There are many variations of this technique, each tailored to the requirements of its application. On production and packaging lines, where large characters and fast print rates are desired, robust solenoid actuated DOD ejectors are used. In photo and document printers, where high resolution and small pixel size are needed, thermal-inkjet (TIJ) and piezoelectric drop ejectors are found. However, these different forms of DOD systems are alike in one aspect. Each method creates a pressure pulse in the fluid reservoir to eject a single droplet of fluid from the orifice. The characteristics of this pulse define the size and velocity of the resulting drop. The varying styles of printers differ only in the method by which this pressure wave is created. Schematics for several of the different forms are shown in Figure 1.2. In piezoelectric ejectors, a PZT actuator is supplied with a large voltage pulse, causing the element to expand and forcing a certain volume out of the orifice. Thermal-inkjet printers rely on a miniature resistive heating element, which, when heated causes the vaporization of a small amount of ink in the reservoir. The formation of this bubble causes a volume of fluid to be expelled from the orifice. Solenoid actuated DOD heads simply use a solenoid valve to briefly connect the flow between a high pressure region and the orifice.

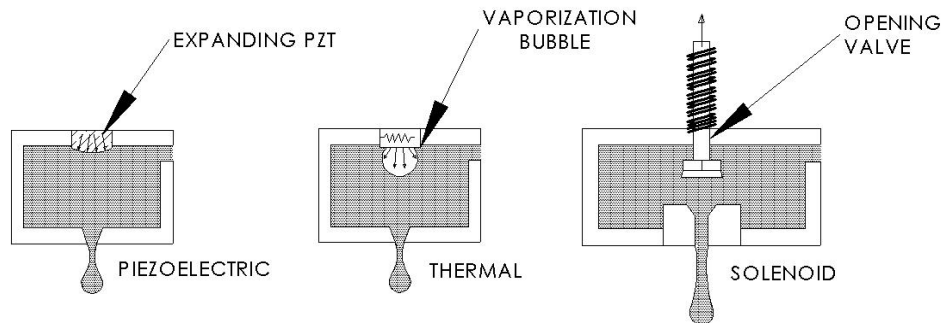


Figure 1.2: Several forms of drop-on-demand ejectors.

Because DOD systems do not alter the droplet trajectories after ejection, drop placement is controlled solely by the positioning of the printer and substrate. Thus, in order to create patterns or characters in an efficient process, large arrays of DOD ejectors are combined in a single print head.

DOD ejectors are capable of producing droplets with diameters less than 10 μ m. However, both the throw distance and versatility of these systems typically decrease with the size of the ejected drops. Also, the droplet formation and flow characteristics at the orifice are highly dependent on the fluid properties of the ink. DOD systems invariably require inks with very low viscosities and particle concentrations. These requirements typically become more stringent as orifice sizes are reduced.

1.2 QUADRUPOLE FOCUSING

The inkjet deposition methods summarized above have been studied thoroughly and continually improved for decades. Photographic and document printers are capable of producing graphics with incredible resolution, while CIJ and various forms of DOD adapt to ever increasing line speeds. However, a fundamental difficulty is encountered when applying these systems to droplet-based fabrication. In particular, the fluid properties, which are suitable for use in an inkjet printer, do not coincide with the ideal properties of a fluid used for fabrication. Inkjet printers generally require inks, which have very low density, viscosity, particle concentration, and particle size. Conversely, an ideal fluid used for fabrication would be a very dense, viscous suspension of large particles. For example, in the case where the element to be manufactured is an electrically conductive trace, the geometry and fluid properties of the droplet on the substrate will define the electrical characteristics of the feature. In particular, the droplet must contain a large enough concentration of conducting particles, such that after evaporation, the particles overlap to form a continuous conducting path. The situation is shown in Figure 1.3 on page 6.

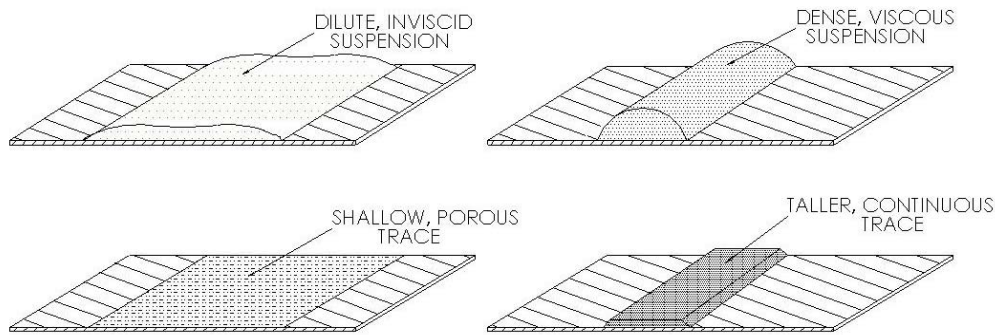


Figure 1.3: Effect of Fluid Properties on Feature Geometry.

If the material has a low surface tension and viscosity and is a dilute suspension of small particles, the droplet will wet the substrate and spread outward. The resulting trace will have a porous structure of a large width and shallow depth. This geometry will produce a feature of poor electrical conductivity and weak abrasion resistance. However, as in the second case in Figure 1.3, if the fluid has a high surface tension, viscosity, and concentration, the result will be a lower aspect ratio, higher density droplet covering less surface area on the substrate. The physical feature created in this case will have a taller, less porous structure, resulting in higher conductivity and improved integrity.

To accommodate the desired material properties at both stages of the process, changes must take place in the droplet after ejection, but before deposition. It is in this direction that the present research is aimed. Because the droplets are exiting the ejector at some velocity, and assuming that a certain amount of time and physical exposure are necessary to invoke a change in the fluid, the droplet will be required to travel some distance. However, because the droplets are subject to irregularities in trajectory, and assuming that they will be exposed to other random forces such as small air currents, it would be impossible to maintain a high resolution in their placement over a certain length. For this reason, some mechanism to control the particle trajectories is needed.

The goal of this study was to investigate the use of a linear electrodynamic quadrupole in focusing such microdroplet streams for deposition.

The linear electrodynamic quadrupole, or mass filter, was developed by W. Paul and his colleagues at the University of Bonn in the early 1950's [1]. The device was created for use in particle physics as a means for determining the charge-to-mass ratio (e/m) of elementary particles. This research also led to the development of the 3-dimensional electrodynamic trap, which has proven invaluable in the observation and measurement of charged particles.

A linear quadrupole consists of four electrodes arranged with their axes at the corners of a square. By connecting the electrodes, as shown in Figure 1.4, and applying an AC voltage across adjacent rods, particles of a certain charge-to-mass ratio are focused to the z-axis as they travel through.

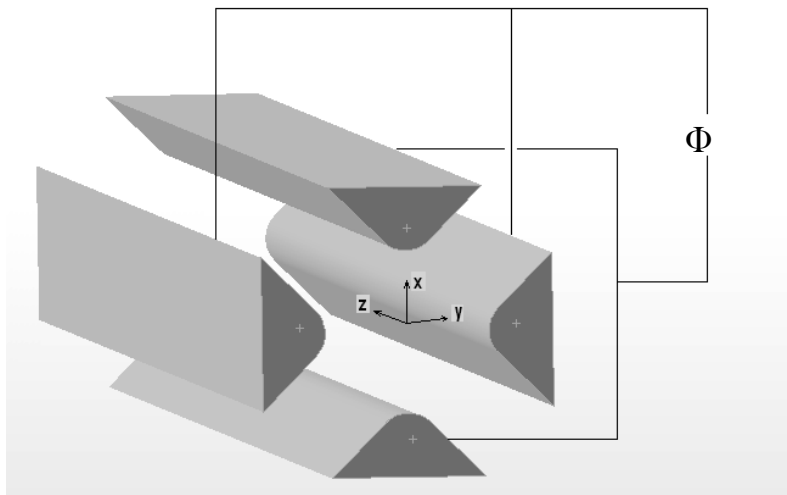


Figure 1.4: Geometry of a linear quadrupole with hyperbolic electrodes.

So, if droplets are ejected along the central axis of the quadrupole and are charged appropriately, the device will constrain their motion in the xy-plane. In this way, the system will allow an interval, in which the properties of the droplets may be altered during their flight. Also in the physical sense, the open geometry of the device allows a space for modification of the droplets. Although this paper is not concerned with the methods or materials employed in this process, several examples of techniques to change the fluid properties are worth mentioning. The simplest method would be the use of resistive heating for the evaporation of the carrying solvent in the droplets. In this case, the starting solution might be a low density, dilute ink solution, suitable for use in the drop ejector, which would then be reduced to a smaller droplet of high concentration upon reaching the substrate. In this way, the resolution and geometry of the resulting physical feature is improved. Another method which might be employed is the use of ultraviolet curing to change the viscosity, concentration, or electrical properties of the drops prior to contacting the substrate.

The inkjet technology used for droplet ejection is also not consequential, as long as the droplets are charged appropriately and ejected along the quadrupole axis. A system consisting of several CIJ printers deflecting droplets of different materials through the quadrupole to allow for the dynamic selection of material can be envisaged.

So, without further consideration of the applications, the goal of this research was to assess the use of a linear quadrupole for controlling the motion of ejected microdroplets. This study was performed with the object of providing a means for modifying the material properties of the droplets after ejection, but before deposition, thus improving their potential for additive fabrication.

2.0 THEORY

2.1 DROPLET CHARGING

The amount of electric charge contained in a droplet is a critical parameter in defining its stability within the quadrupole device. Thus, adequate measurement and control of this quantity are necessary for reliable operation.

2.1.1 Fluid Jet Polarization

In charging droplets of a fluid with high electrical conductivity, the most commonly used practice is that of fluid jet polarization [2]. In this method, electrodes are placed in such a way that an electric field exists across the point of droplet formation. The situation is shown in the schematic of Figure 2.1.1.

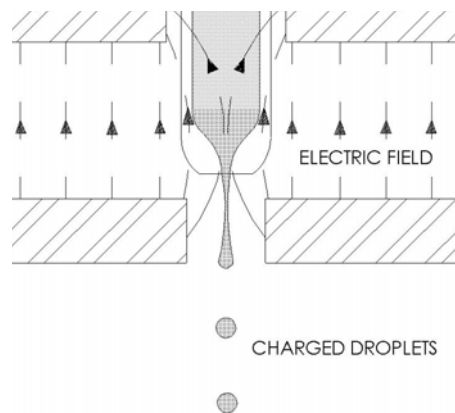


Figure 2.1.1: Droplet Charging with Fluid Jet Polarization.

As the flow passes through the electrodes, and a droplet begins to form, the electric field causes a charge gradient in the fluid column. Then, as the droplet cleaves, it retains a portion of this charge imbalance. By adjusting the potential applied to the electrodes, and thus, the magnitude of the electric field, the overall charge of the ejected droplets can be controlled.

2.1.2 Rayleigh Instability

The maximum charge that a droplet can hold is defined by the droplet radius and surface tension of the fluid. Above this limit, the electrostatic repulsion of the like charges residing on the surface of the droplet overcomes the inward force due to the surface tension of the fluid, and the droplet disintegrates into at least two smaller droplets [3], [4]. For a drop of radius a_0 and surface tension γ , the inequality, expressed in terms of the fissility ratio X , can be written

$$X = \frac{Q^2}{64\pi^2 \epsilon_0 \gamma a_0^3} < 1. \quad (2.1.1)$$

This coulomb instability will have a detrimental effect on the focusing properties of the quadrupole. So to maintain a high resolution system, care must be taken to avoid the Rayleigh limit (Equation 2.1.1). Because the radius of the droplets will decrease due to evaporation, as they travel through the device, the fissility ratio will increase with time. Therefore, the applied charge must be low enough that the Rayleigh limit is not approached during the time of flight.

2.1.3 Electrostatic Deflection

The force on a droplet in a uniform electric field is directly proportional to the field strength and to the magnitude of charge residing on the drop. The motion of the droplet in the direction of the electric field will then be defined by its mass and an external viscous drag force due to the surrounding medium. The force balance for a droplet moving in air through parallel capacitor plates gives

$$x'' + \frac{6\pi\mu a}{m} x' = \frac{V}{md} q \quad (2.1.2)$$

Where the drag force is estimated by Stoke's Law (see Section 2.2), and V , d , and m are the voltage applied to the capacitor plates, distance between plates, and droplet mass, respectively. This relation was used to determine the value of electric charge on ejected droplets, according to the field strength applied across the point of droplet breakup.

2.2 FLUID FLOW

The fluid flow problem for this application is commonly encountered in engineering practice. After a fluid droplet is released from the piezoelectric drop generator, it takes a spherical shape and falls under the influence of gravity. For Reynolds numbers of $Re \ll 1$, the inertial terms in the Navier-Stokes equations can be neglected and the analysis is simplified immensely. Following the traditional derivation for this problem, the no-slip boundary conditions were applied to the surface of the sphere, and the far field boundary conditions of $U_F \rightarrow 0$ as $r \rightarrow \infty$ were used.

From this derivation, the viscous drag force due to the surrounding fluid is found to be

$$F_d = -6\pi\mu_2 aU, \quad (2.2.1)$$

where U is the droplet velocity, μ_2 is the viscosity of air, and a is the droplet radius. This is the well known Stoke's Law [5], [6]. The only other force acting on the droplet in the z-direction is that of gravity, which, allowing for the buoyant force of the surrounding air, can be written

$$F_g = \frac{4}{3}\pi a^3 g(\rho_1 - \rho_2), \quad (2.2.2)$$

where ρ_1 and ρ_2 are the density of the droplet and air respectively. The terminal velocity for a body falling through a viscous medium is obtained simply by setting the drag force equal to the gravitational body force. From equation (2.2.2),

$$U_t = \frac{2a^2 g(\rho_1 - \rho_2)}{9\mu_2} \quad (2.2.3)$$

This formula is valid for fluid droplets of diameters as low as 20 μm . For droplets below this range, an error is incurred due to the continuum assumption and a correction factor must be included [7]. However, for the calculations presented here, equation (2.2.3) is sufficient.

Applying the law of inertia to the droplet and rearranging terms, gives the following equation of motion in the z-direction:

$$m \frac{d^2 z}{dt^2} + 6\pi\mu_2 a \frac{dz}{dt} = \frac{4}{3} \pi a^3 \rho_1 g \quad (2.2.4)$$

Then defining the relaxation time as $\tau = \frac{2a^2 \rho_1}{9\mu_2}$, the differential equation for particle motion

becomes

$$\tau \frac{d^2 z}{dt^2} + \frac{dz}{dt} = \tau g. \quad (2.2.5)$$

Setting the origin at the entrance to the device and applying the initial conditions

$$w(0) = w_0, \quad z(0) = 0,$$

yields the exact solution

$$z = \tau g t + \tau (w_0 - \tau g) \left(1 - e^{-\frac{t}{\tau}} \right). \quad (2.2.6)$$

This solution provides an initial estimate of the droplet progression in the z-coordinate direction with time. In the present case, however, the assumption that $\text{Re} \ll 1$ is not always valid.

Depending on the characteristics of the drop generator, the initial droplet velocities can be high, and the resulting Reynolds numbers of the flow can reach $\text{Re} = 5$. For this reason, Oseen's solution is used, ignoring terms of $O[\text{Re}^2]$ and higher, to define the drag force as

$$F_d = -6\pi\mu_2 a \frac{dz}{dt} \left(1 + \frac{3}{16} \text{Re} \right). \quad (2.2.7)$$

Because the particle is a fluid sphere, the no-slip condition, applied to the surface of the particle in the derivation of Stokes Law, does not hold. In this case, the modified drag force due to the circulation of the fluid within the droplet is given by

$$F_d = -6\pi\mu_2 a \frac{dz}{dt} \left(1 + \frac{3}{16} \text{Re} \right) \left[\frac{3(\mu_1 + \mu_2)}{(3\mu_1 + 2\mu_2)} \right]. \quad (2.2.8)$$

However, this relation reduces to (2.3) for the case of $\mu_1 \ll \mu_2$ [3]. A more accurate equation of motion in the vertical coordinate direction for the falling droplet is then

$$m \frac{d^2 z}{dt^2} + 6\pi\mu_2 a \frac{dz}{dt} \left(1 + \frac{3}{16} \text{Re} \right) = \frac{4}{3} \pi a^3 g (\rho_1 - \rho_2). \quad (2.2.9)$$

Because the solvent of the droplet is evaporating as it travels through the device, the density and radius are both functions of time. To consider these variables as time dependent, the equation of motion is integrated numerically (see Section 3.3).

2.3 QUADRUPOLE FOCUSING

2.3.1 The Quadrupole Electric Field

In a quadrupole field, the force on a charged particle increases as the particle moves away from the null point. For a perfect field, the magnitude of the force on the particle is defined by a linear dependence on position. Following the derivation of Dawson, the field can be expressed as

$$E = E_0 (Ax + By + Cz), \quad (2.3.1)$$

where A , B , and C are constants and E_0 is position independent, but may be a function of time.

Applying Laplace's equation gives (2.3.2)

$$\nabla \cdot E = A + B + C = 0.$$

To satisfy this relation the values $A = -B, C = 0$ are used. Then, substituting these values and integrating (2.3.1) gives the following expression for the electric potential.

$$\Phi = -\frac{1}{2} E_0 A (x^2 - y^2) \quad (2.3.3)$$

The equipotential lines of this field are sets of rectangular hyperbolae with four-fold symmetry in the xy plane, as shown in Figure 2.3.1, below.

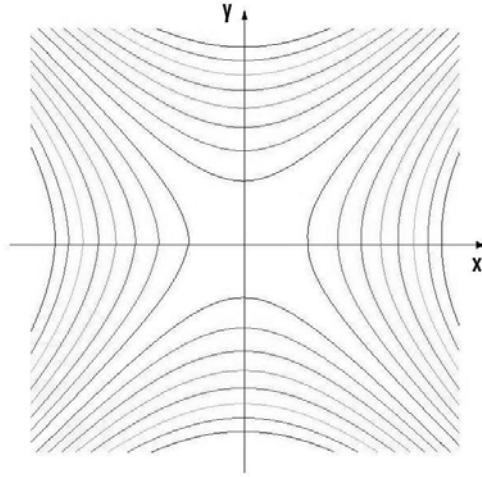


Figure 2.3.1: Equipotential curves of a quadrupole field.

To create this field, the electrodes must have an internal surface, which follows one of these sets of hyperbolic curves. The boundary conditions are then met by assuming that the potential is constant over the electrode surface. If the closest distance between opposite electrodes is r_0 , and the potential applied between adjacent electrodes is Φ_0 , the electric potential for the field can be written

$$\Phi = \Phi_0 \frac{(x^2 - y^2)}{2r_0^2}. \quad (2.3.4)$$

From this relation it can be seen that for a given value of Φ_0 , a charged particle in this field will be deflected toward the central axis in one coordinate direction and away from the axis in the other direction. Therefore, in order to hold a particle within the field, Φ_0 must be a periodic function in time. The particles will then be alternately deflected toward and away from the central axis in each coordinate direction. If the particles have a large enough mass that they are

not deflected out of the device during the defocusing part of the cycle, a periodic stability can be created [1]. The form of the potential Φ_0 , which will be chosen, is a sinusoidal voltage of zero to peak amplitude V and angular frequency ω .

2.3.2 Equations of Motion

The motion of a charged particle, in the electric field described above, will be defined by the magnitude and frequency of the driving voltage. However, its motion will also be affected by a viscous drag force, proportional to its velocity, and acting in the opposite direction. If it is assumed that the particle is spherical and the velocities in the x and y -coordinate directions are in the Stoke's regime, the drag force is

$$F_D = 6\pi\mu R \frac{du}{dt}, \quad (2.3.5)$$

where $u = x, y, z$, R is the particle radius, and μ is the viscosity of air.

Then, assuming that the z -axis is parallel to the direction of gravity, and balancing the forces gives the following equations of motion for a charged particle in the linear quadrupole:

$$\begin{aligned} m \frac{d^2 x}{dt^2} + 6\pi\mu R \frac{dx}{dt} - \left(\frac{eV}{r_0^2} \cos \omega t\right)x &= 0 \\ m \frac{d^2 y}{dt^2} + 6\pi\mu R \frac{dy}{dt} + \left(\frac{eV}{r_0^2} \cos \omega t\right)y &= 0 \end{aligned} \quad (2.3.6)$$

After substituting $\xi = \frac{\omega t}{2}$, $K = \frac{6\pi\mu R}{m\omega}$, and $q = \frac{2eV}{m\omega^2 r_0^2}$, these equations can be written

$$\begin{aligned} \frac{d^2 x}{d\xi^2} + 2K \frac{dx}{d\xi} - (2q \cos 2\xi)x &= 0 \\ \frac{d^2 y}{d\xi^2} + 2K \frac{dy}{d\xi} + (2q \cos 2\xi)y &= 0 \end{aligned} \quad (2.3.7)$$

2.3.3 Stability

The stability of charged particle trajectories in quadrupole fields has been thoroughly studied for use in mass spectrometry and is well understood. The motion of an ion in a linear quadrupole mass filter is described by the Mathieu equation [8]. This equation, in its canonical form, is given as

$$\frac{d^2u}{d\xi^2} + (a_u - 2q \cos 2\xi)u = 0 \quad (2.3.8)$$

where u represents either x or y ,

$$a_u = a_x = -a_y = \frac{4eU}{m\omega^2 r_0^2}, \quad q = q_x = -q_y = \frac{2eV}{m\omega^2 r_0^2},$$

and U is a direct voltage component applied across the common electrodes as shown in Figure 2.3.1.

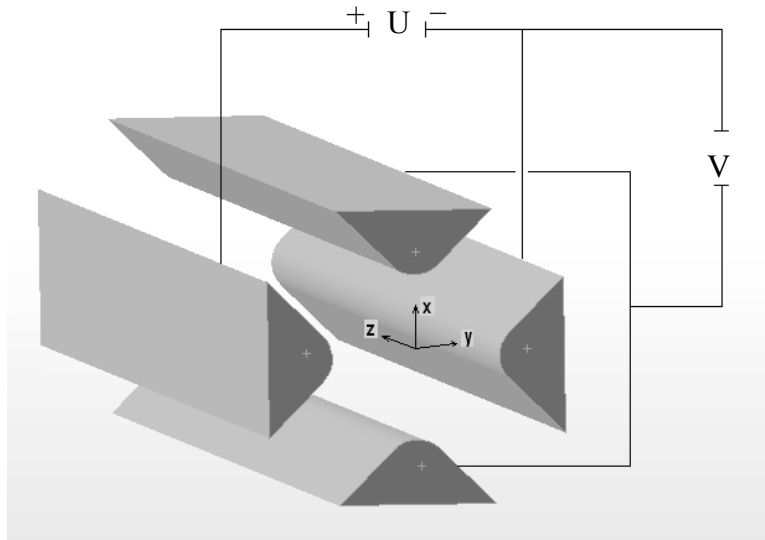


Figure 2.3.2: Schematic of a Linear Quadrupole Mass Filter.

The function of this DC voltage is to cause heavier ions to become unstable and exit the apparatus while lighter ions are able to follow the AC voltage and pass through. Using a combination of alternating and direct voltage components, the device then acts as a band-pass mass filter. The solutions to equation (3.8) can be expressed by

$$u = \alpha' e^{\mu\xi} \sum_{n=-\infty}^{\infty} c_{2n} e^{2in\xi} + \alpha'' e^{-\mu\xi} \sum_{n=-\infty}^{\infty} c_{2n} e^{-2in\xi} . \quad (2.3.9)$$

The derivation of this equation and the calculations of the constants are not pertinent to the goal of this thesis. Only the nature of the solutions and approximate bounds for stability are desired. The parameters α' and α'' are integration constants depending on the initial phase, position, and velocity. The constants C_{2n} and μ depend on the values of a and q and not upon the initial conditions [1]. Therefore, the nature of ion motion inside the quadrupole depends solely on the values a and q . From this, we find that all ions with the same charge-to-mass ratio will have the same periodicity of motion and thus the same stability properties in the device for a certain set of driving voltages. The conditions for stability can then be mapped in the a - q plane. Figure 2.3.2 shows a representative plot of the first simultaneous stability region for both coordinate directions. By selecting a certain a/q ratio, one can define an operating line for mass filter operation which will only allow ions with a given m/e ratio to pass through [1].

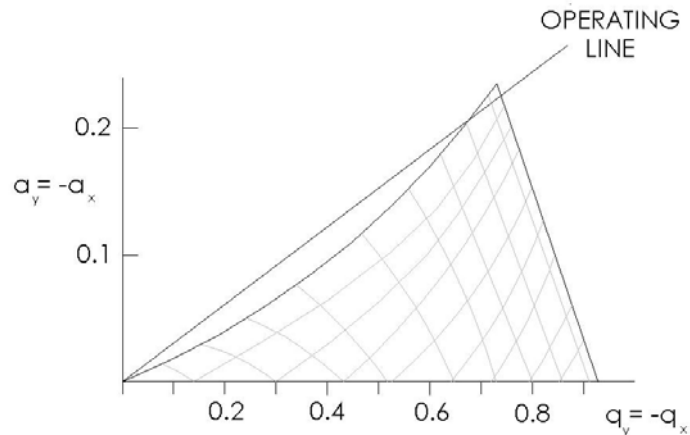


Figure 2.3.3: The lower stability region usually used in mass filter operation.

However, for the use of the linear quadrupole as a focusing device, the consideration of an a/q ratio is not necessary. Because there is no direct voltage component, the stability region in Figure 2.3.2 is the q -axis for $q < 0.91$. But if we interpret the parameter a in a different regard, namely as an arbitrary defocusing force, we see that the strongest focusing effect occurs at the tip of the stability diagram (at $q = 0.706$). Thus the optimal value and upper limit for q are obtained from the theory of quadrupole spectrometry.

It should be noted that the viscous drag force on the particle was not considered in equation (3.8). As presented by McLachlan [9], the substitution can be made in equation (3.7)

$$u = u_1 e^{-K\xi},$$

where u is either x or y . Substituting and canceling $e^{-K\xi}$ gives

$$\frac{d^2 u_1}{d\xi^2} + (b - 2q \cos 2\xi) u_1 = 0, \quad (2.3.10)$$

where

$$b = a - K^2 = \frac{4eU}{m\omega^2 r_0^2} - \left(\frac{6\pi\mu R}{m\omega} \right)^2.$$

This is again the general form of the Mathieu equation and the solutions approach zero for $0 < \mu < K$ as $e^{(\mu-K)\xi}$ for increasing ξ . Therefore, the viscous damping term expands the stability boundaries out to $\mu = k$ [10].

3.0 NUMERICAL CALCULATIONS

3.1 PARTICLE TRAJECTORIES

Although the Mathieu equation provides valuable information on the stability characteristics of the device, it is not practical for calculating particle trajectories. The Mathieu equation and the stability map are only defined in the neighborhood of the z-axis [11]. Therefore, using this equation, we are not able to consider the case of significantly off-axial initial conditions. Practically, it will not be possible to inject particles at exactly the null point or perfectly parallel to the z-axis. In order to analyze the restoring rate of the device for these situations, the particle trajectories were obtained numerically by direct integration of the equations of motion with the fourth-order Runge-Kutta method. First, the equations (3.7) are expressed in dimensionless form as

$$\begin{aligned}\frac{d^2 x_*}{d\xi^2} + 2K \frac{dx_*}{d\xi} - (2q \cos 2\xi)x_* &= 0 \\ \frac{d^2 y_*}{d\xi^2} + 2K \frac{dy_*}{d\xi} - (2q \cos 2\xi)y_* &= 0\end{aligned}$$

where $x_* = \frac{x}{r_0}$ and $y_* = \frac{y}{r_0}$.

By integrating these equations, and approximating the expected values of the constants and initial conditions, a plot, as shown in Figure 3.1.1, is obtained. The example shown is in dimensional form and gives the progression of the particle trajectory in the x-coordinate direction with respect to time. The entry point is 0.1mm off-axis, and the particle has an initial velocity of 0.001m/s in the positive x-direction.

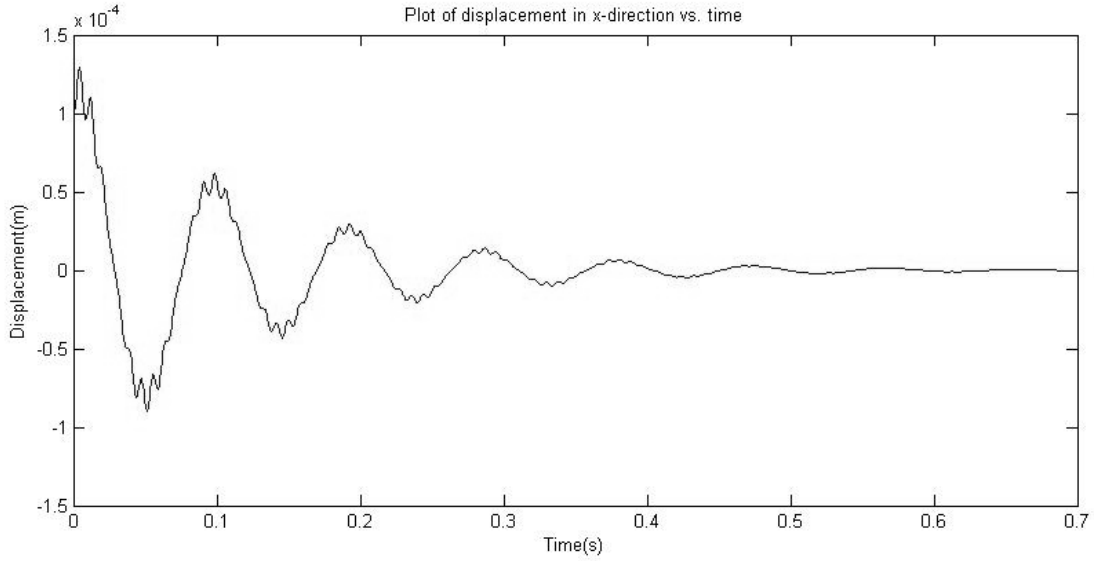


Figure 3.1.1: Particle trajectory in x-direction for: $\omega = 400$, $a = 40\mu\text{m}$, $r_0 = 1.38\text{mm}$.

This solution is valid for a solid, spherical particle of constant mass and volume falling through the quadrupole mass filter. As can be seen in the figure, the particle oscillates about the z-axis with exponentially decreasing amplitude. This is true for all situations where the parameter q_z is within the stability bounds. There are two frequencies associated with the motion, both of which are dependent on the applied potential frequency, ω , and the charge to mass ratio of the droplet. The secondary oscillation, of lesser amplitude, has the same frequency as the AC driving voltage itself. The frequency of the larger oscillation, however, decreases in magnitude when the frequency of the applied potential ω , is increased. This trend is shown in the plots of Figure 3.1.2, where the particle trajectories are given in terms of the dimensionless parameter x^* .

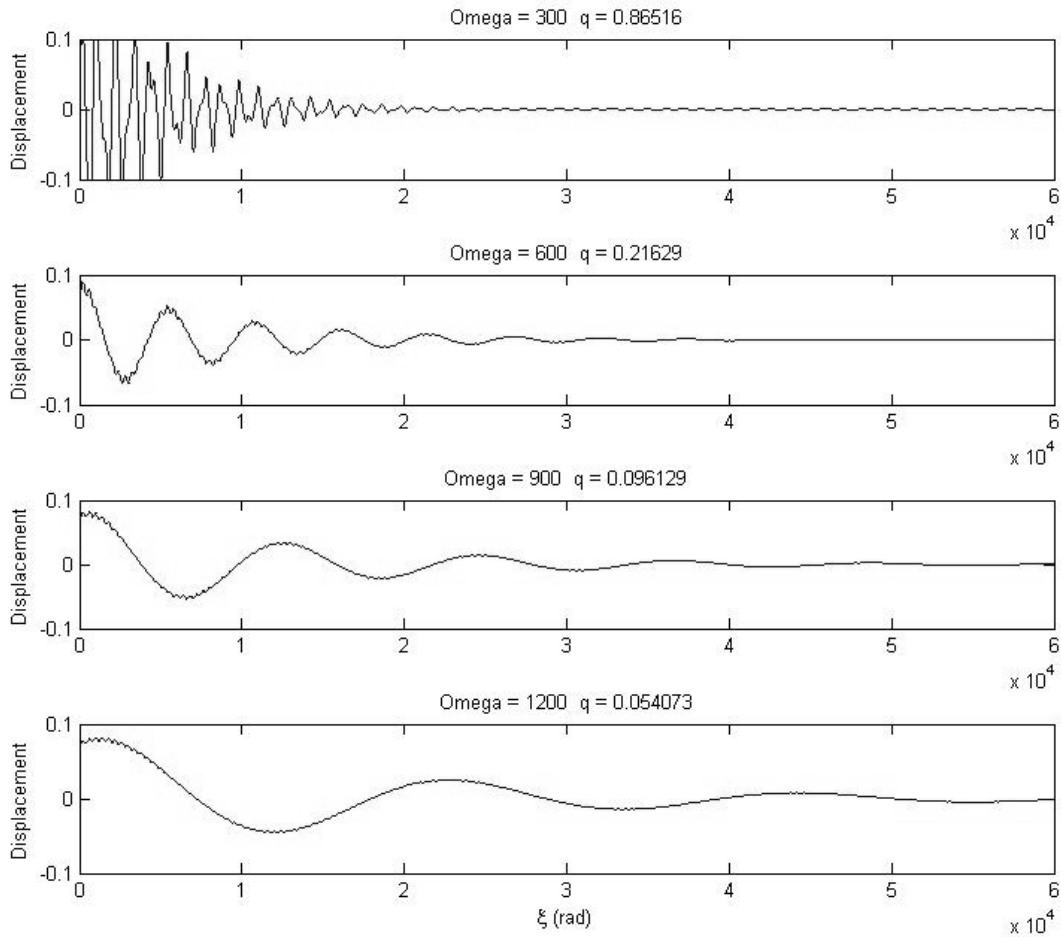


Figure 3.1.2: Particle trajectories for several values of q .

It can be seen that as the value of q is increased, the two frequencies approach one another, and the motion becomes less stable. This is intuitive, when the definition of the parameter q is considered. This variable is proportional to the charge on the particle and to the amplitude of applied voltage. If either of these quantities is increased, the particle experiences larger accelerations and is better able to follow the applied voltage. So, from these plots, it appears that the stability of the system is increased with decreasing values of the parameter q . However, there are other factors that must be considered before an optimal value of q is chosen. Figure

3.1.3, below, shows the restoring rate for a range of q values. The restoring time for this case has been defined as the time taken for the system to reduce the maximum off-axial amplitude to less than 0.005% of the quadrupole radius.

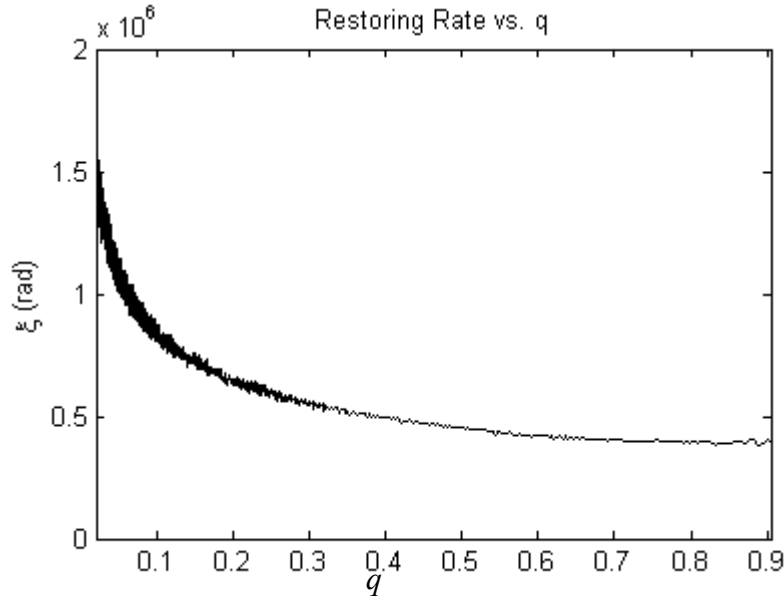


Figure 3.1.3: Restoring rate in terms of the number of oscillations of the field.

As stated in Section 2.3.1, a charged particle in a quadrupole field will experience a force in the plane normal to the rods, directly proportional to the magnitude of the electric field at that point. This force will tend to push the particle toward the origin in one coordinate direction and away from the origin in the other direction. However, if the voltage potential applied to the rods is periodic in time, the particle will be forced sequentially toward and away from the origin in both coordinates. From the plots of particle trajectories, it is evident that for each cycle of the quadrupole field, there is a net force, restoring the particle to the z-axis.

The plot of Figure 3.1.3 shows that the number of cycles of the field necessary to focus the particle within a given bound increases as the value of the parameter q is reduced for $q < 0.7$. This means that the net force toward the z -axis over each oscillation of the electric field increases as q is increased and reaches a maximum at $q \approx 0.7$.

To further investigate the characteristics of this net repressive force, the effect of the initial conditions must be considered. All of the results presented thus far have been calculated with a certain set of off-axial initial conditions x_0 , u_0 , and φ_0 . These are the initial x -coordinate position, initial velocity in the x -direction, and initial phase, respectively. If the initial velocity in the positive x -direction is increased, while the other variables are left unchanged, the results give a similar trend to that presented above. Figure 3.1.4 shows the maximum displacement from the z -axis experienced by a particle as it travels through the device for a range of AC potential frequencies. In this case, higher frequencies in the applied potential and thus, smaller values of q , result in larger displacements of the particle from the z -axis. The line superimposed at $x^* = 1$, on the plot of the particle displacement in Figure 3.1.4 represents the radius of the linear quadrupole. When a droplet deviates past this limit, it will collide with the quadrupole rods and be lost. Therefore, this value provides a lower limit on the parameter q for a given set of initial conditions. As expected, the upper limit for q occurs at $q \approx 0.90$, above which, all trajectories diverge from the z -axis. So, for example, in this case of significantly off axial initial conditions, the range of possible q values becomes $0.04 < q < 0.90$.

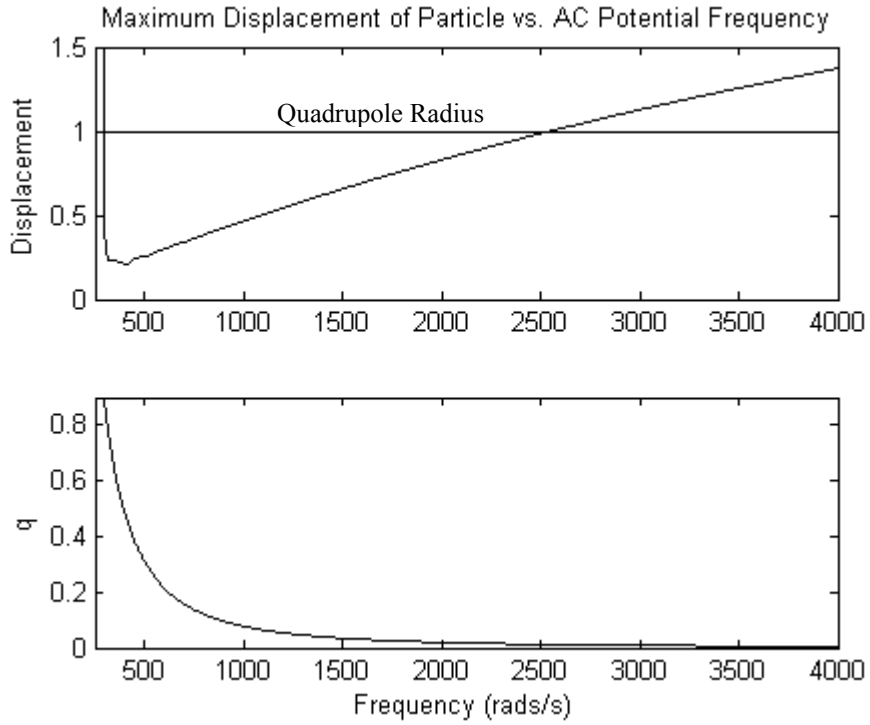


Figure 3.1.4: Maximum displacement experienced by a particle for different values of q .

It can also be seen in Figure 3.1.4, that a minimum value in the plot of maximum oscillation amplitudes is observed for the conditions where $q \approx 0.7$. This value agrees with the approximation for the maximum restoring force of Figure 3.1.3 and the theoretical value predicted in section (2.3.3). Figure 3.1.5 below, shows the maximum displacement x_* , experienced by particles for several off-axial initial velocities.

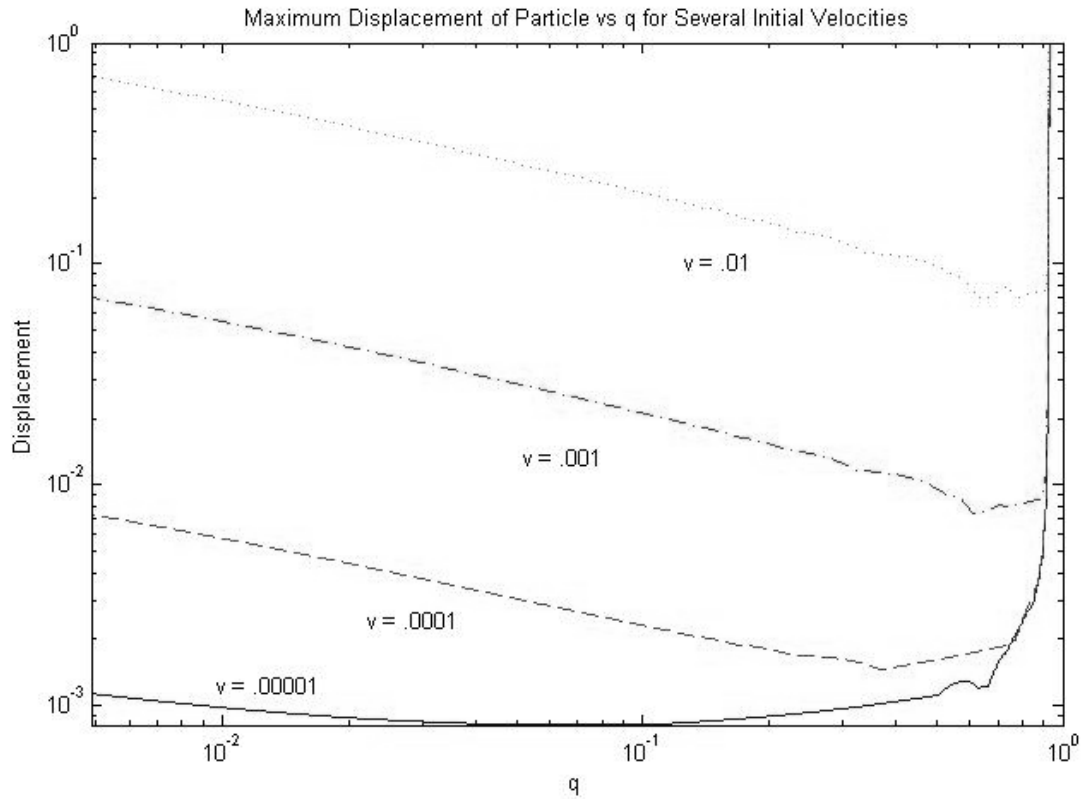


Figure 3.1.5: Maximum displacement of a particle for several initial velocities.

It can be seen that for large initial velocities in the off-axial direction, the maximum displacement of the particle increases with decreasing values of q . Conversely, for smaller initial velocities, the maximum displacement decreases with decreasing values of q . This incongruity can be attributed to the initial phase of the voltage potential. The largest amplitude of oscillation is observed when the droplet enters the device with an initial velocity in a given off-axial direction and the phase of the applied potential is such that the induced field exerts a force on the drop in this same direction. This is the effect that is observed in the plot of Figure 3.1.5. For the case of large initial velocities and a large value of q , the momentum of the particle is counteracted quickly by the electric field. As the values of q are reduced, the accelerations due to the field are also reduced, and the momentum of the particle carries it to larger maximum amplitudes. In the case of a small initial velocity, however, increased values of q will result in

larger initial displacements when the initial phase of the electric field is adding to the particle momentum. Figure 3.1.6, below gives the maximum off-axial amplitudes of droplets for the same conditions as those used in Figure 3.1.5, but with an initial phase differing by $\pi/2$ radians.

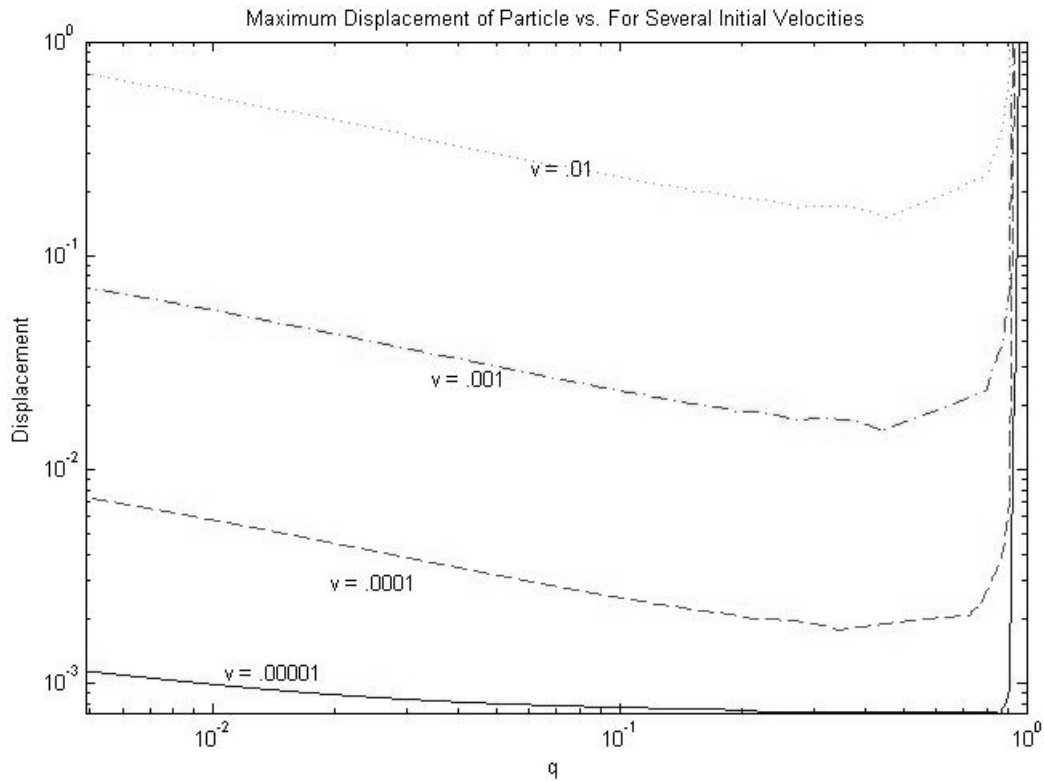


Figure 3.1.6: Maximum Displacements for several different initial velocities and an initial phase of $\phi = \pi / 2$.

In this figure, the displacements follow the expected trends more closely. It is evident, however, that for q values from $0.1 < q < 0.8$, the maximum amplitudes remain fairly constant.

Another aspect, which must be explored before choosing an optimal value of q , is the focusing rate of the device in real time. In Figure 3.1.3, the restoring rate was considered with respect to

the number of oscillations of the field. However, because the frequency of the applied potential defines these oscillations, it is reasonable to presume that it will also control the focusing rate. In Figure 3.1.7, the focusing time, defined as the time (in seconds) required for the system to reduce the maximum off-axial amplitude to less than 0.005% of the quadrupole radius, is plotted against the frequency of the driving voltage for several initial velocities.

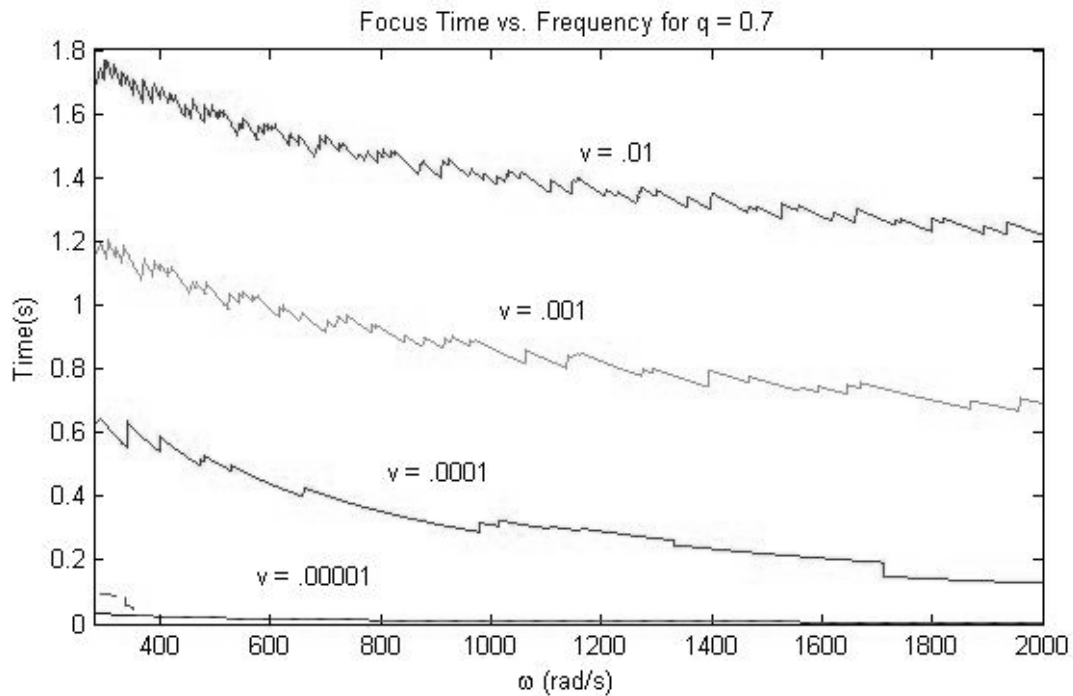


Figure 3.1.7: Focusing time for several initial conditions.

The observable trend in this figure is that for a given value of q , the time required for confining the amplitude of a particle within some bound, from off-axial initial conditions, decreases for increasing frequency of the applied AC potential. Also, as would be expected, the focusing time decreases with reductions in the magnitude of initial off-axial displacement and velocity.

3.2 DROPLET EVAPORATION

The results presented above are valid for the motion of a solid spherical particle of constant mass traveling through the device. For the case of a fluid droplet falling through the quadrupole field, the situation is much more complex. Heat, mass, and momentum transfer between the droplet and air are coupled to define the evaporation rate. The droplet mass and radius are then decreasing functions of time, dependent on the surroundings. The physics of an evaporating multi-component droplet moving through a viscous medium presents a very complex problem that is beyond the scope of this paper. However, the response to both the viscous drag force and the electromotive force are dependent on the droplet radius and mass. In order to approximate the changing radius, which is essential for determining the trajectories, the well known “ a^2 versus time law” for quasi-steady state droplet evaporation was used [3]. The simplest form of this relation can be expressed as

$$a^2 = a_0^2 - \beta(t - t_0) \quad (3.2.1)$$

where, a is the droplet radius and β is a time independent parameter. The values of β used in the calculations were determined by experiment. As the solvent of the droplet evaporates, the concentration of the contained solids increases accordingly, and the mass of the system decreases by the relation

$$m = m_u + m_s = \frac{4\pi}{3} \left(c_0 \rho_u a_0^3 + \rho_s [a_0^2 - \beta(t - t_0)]^{\frac{3}{2}} \right). \quad (3.2.2)$$

To account for the changing mass and radius in the numerical calculations, these values were updated during each time step in the Runge-Kutta algorithm. From a focusing standpoint, the decreasing mass and radius of the droplet both act to increase the q value with time. Therefore, the stability properties of the droplet will change as it travels through the device, and, if the operating variables are not well chosen, its motion in the xy-plane will not be constrained. An example trajectory in the x-direction for an evaporating droplet traveling through the device is shown in Figure 3.2.1.

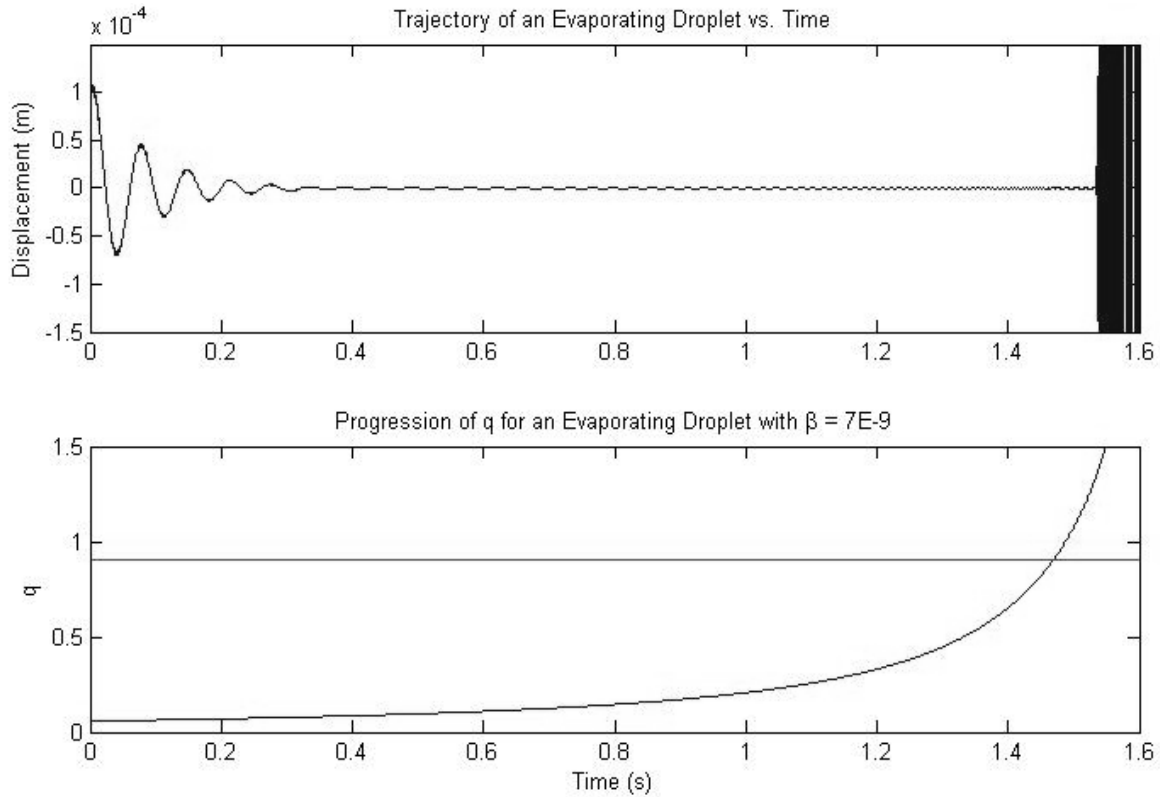


Figure 3.2.1: Trajectory and changing value of q for an evaporating droplet.

As can be seen in the plot, the droplet begins at an off axial initial position, is focused and held near the z -axis, and then eventually diverges. The second plot in this figure shows the changing values of q as the droplet evaporates. The line superimposed on this plot is the theoretical stability boundary at $q \approx 0.905$. While q is within the stable region, the oscillation amplitudes of the droplet decrease exponentially about the z -axis. The nature of the motion during this focusing portion of the process follows the same trends as those observed for a solid particle. One difference due to the increasing value of q , however, is that the frequency of oscillation about the z -axis increases with time. As q approaches the instability limit, this frequency approaches that of the applied potential, and an exponential increase in the oscillation amplitudes

ensues. In Figure 3.2.2, looking more closely at the onset of instability, there appears to be some lag time from when the upper limit for q is reached and when the droplet begins to depart from the central axis.

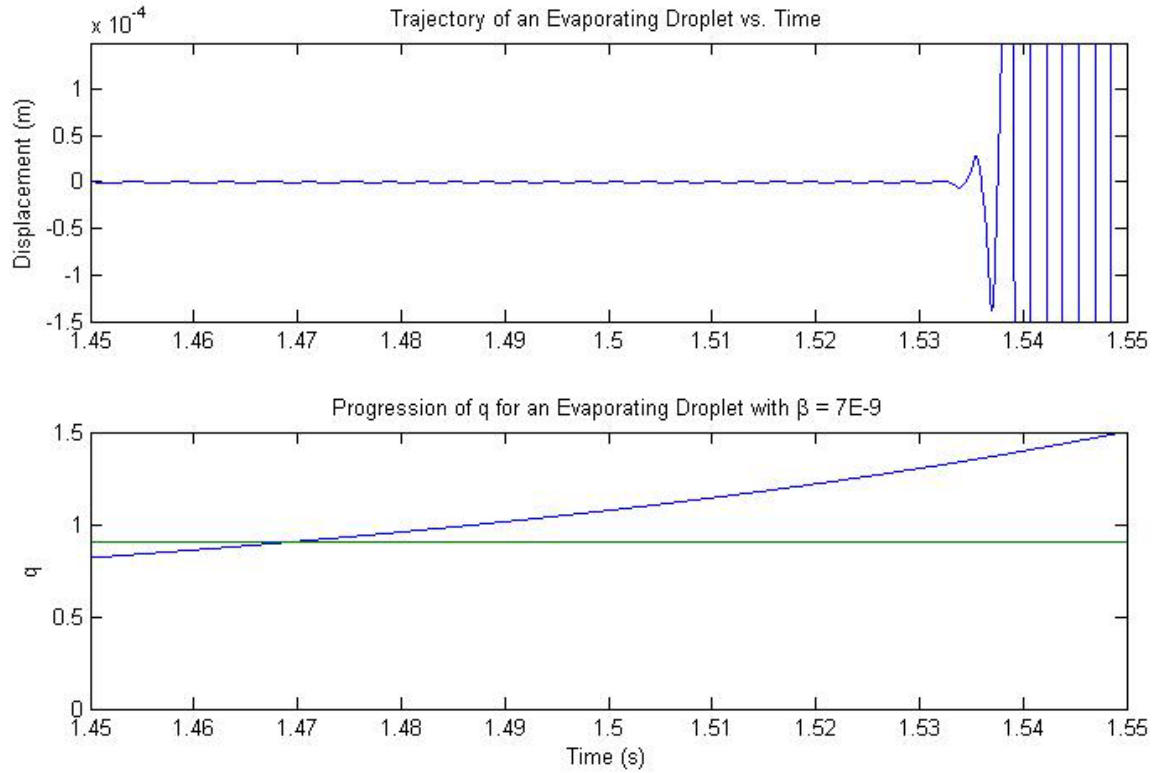


Figure 3.2.2: Divergence of an evaporating droplet from the quadrupole.

However, because the droplet does not simply diverge from the axis when the stability limit is reached, but continues oscillating with exponentially increasing amplitudes, the observed inconsistency is due only to the visible range of the plot. And indeed, if the absolute values of displacement amplitudes are graphed on a logarithmic scale, as in Figure 3.2.3, below, it is evident that the inflection point in the data corresponds to the stability limit.

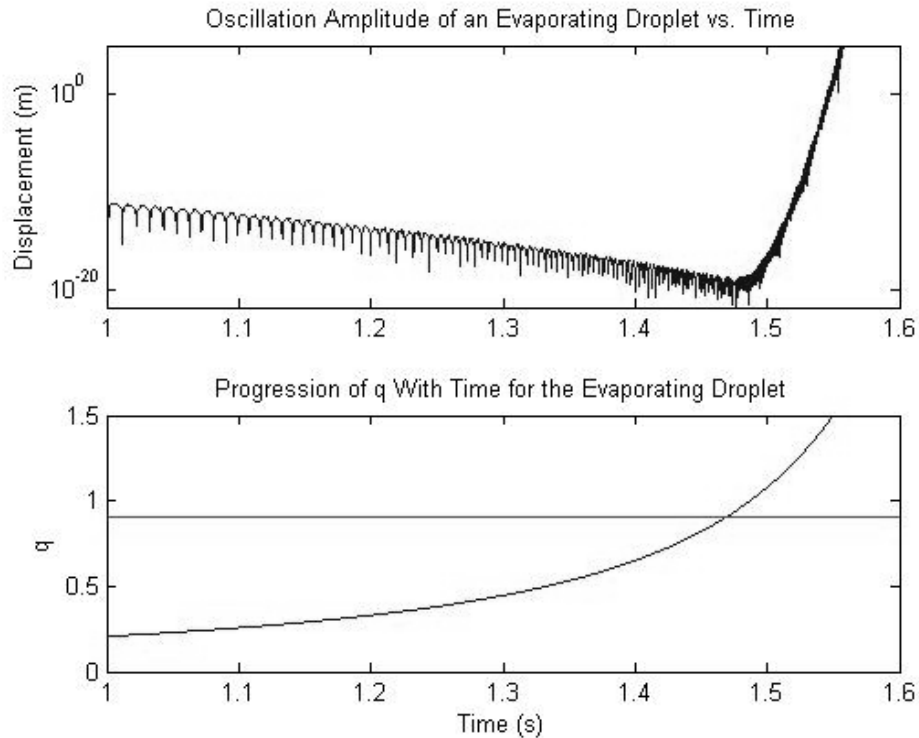


Figure 3.2.3: Oscillation amplitudes for a diverging trajectory.

3.3 VERTICAL MOTION

As previously stated, the theoretical solution, given in Equation 2.2.6, does not provide an accurate representation of the droplet motion in the vertical direction for the initial high-velocity interval. This solution also assumes that the droplet density and radius remain constant throughout the period of travel. To obtain a more accurate estimate of the droplet position with time, the modified equation of motion (Equation 2.2.9) with Oseen's approximation is used. A solution to this equation, allowing for the changing density and radius, is found numerically with the Fourth-Order Runge-Kutta method. Figure 3.3.1 below, shows the predicted particle motions for several different values of the constant β , used in the approximation for the changing radius (Equation 3.2.1).

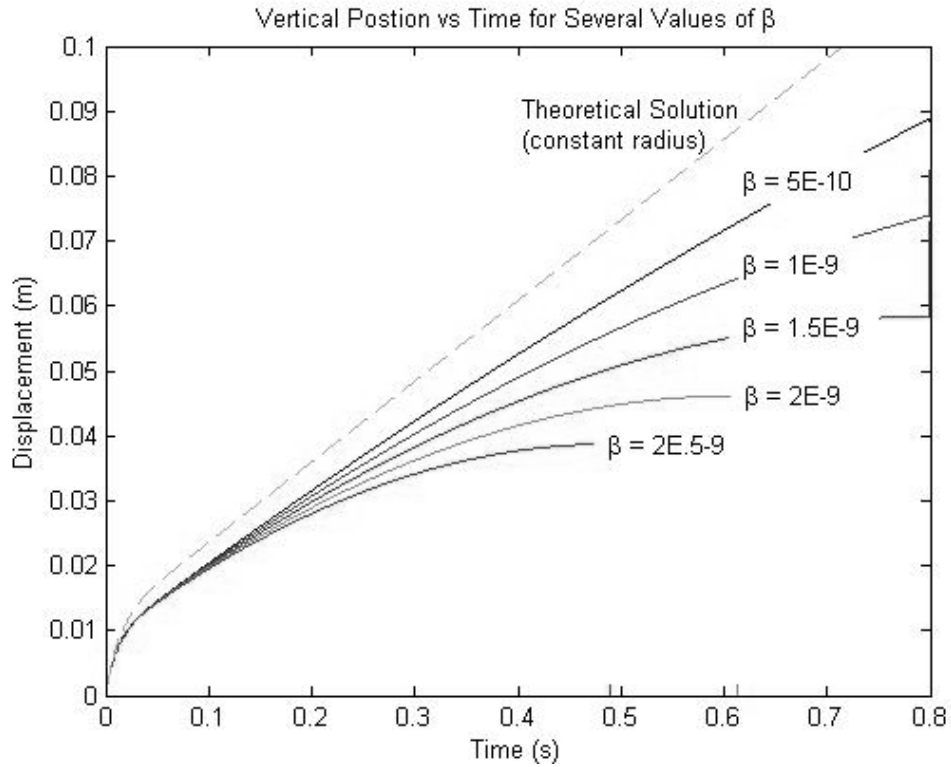


Figure 3.3.1: Plot of vertical position for an evaporating droplet.

As expected, the theoretical solution becomes linear after the initial relaxation time, predicting a constant terminal velocity. The numerical solution gives a larger drag force and therefore a shorter relaxation period, but the velocity in this case continues to decrease with time. It can be seen that the evaporation rate of the droplet has a large impact on its motion within the device; and therefore, accurate measurement of this quantity is necessary before a set of operating conditions can be chosen.

4.0 EQUIPMENT AND SETUP

4.1 DROPLET EJECTION

As mentioned in Section 1.3, the method by which the droplets were created for these experiments was not important to the end goals of the research. However, for simplicity, a piezoelectric DOD system was used. The drop ejector, purchased from Microfab Corporation, was a model MJ-AB-01-40 dispensing valve. The nozzle and orifice were formed by precision grinding of the conical-terminated, closed end of a heat-pulled glass pipette. The resulting orifice was 40 μ m in diameter. An image and schematic of the drop ejector are given in Figure 4.1.1, below.

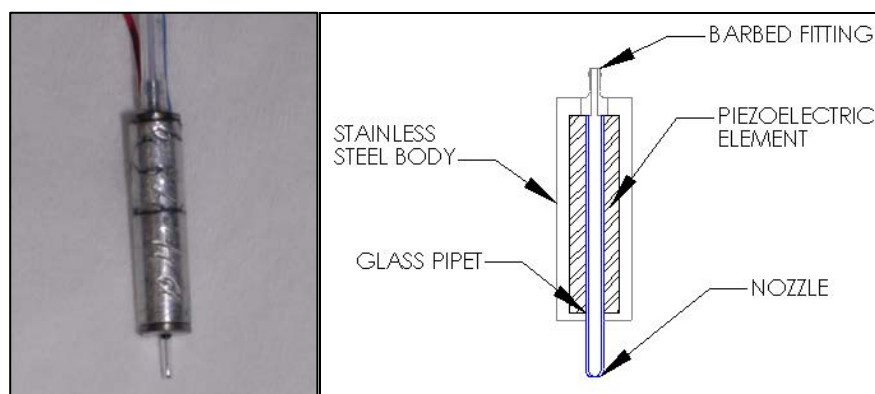


Figure 4.1.1: Image and schematic of the piezoelectric drop generator.

For drop ejection, the pipette was fitted with a radially-polarized, annular piezoelectric element. When a potential is applied to this element, it compresses the glass pipette with a force proportional to the voltage, causing fluid to be ejected from the orifice. Thus, by controlling the PZT with a voltage pulse of a certain magnitude and duration, individual droplets can be formed. A laptop computer and National Instruments DAQ6715 analog output card were used to create the voltage signals. The pulses were amplified with an OPA541 operational amplifier in a non-inverting configuration before being sent to the drop generator.

In a piezoelectric printer, the characteristics of the droplets are defined by the voltage drive signal and the internal system pressure. As presented by E. Lee and colleagues, a vacuum pressure applied to the ink reservoir is necessary to prevent the ink from wetting the outer surface of the orifice and impairing droplet formation [2]. This negative pressure was created with a Cole Parmer 74900 series syringe pump fitted with a 10cc plastic syringe. An ACSI digital vacuum pressure gauge was used to monitor the reservoir pressure. An inline filter with a 5 μ m pore size was used to remove agglomerates and other particles that would potentially clog the orifice.

In order to ensure proper axial alignment with the other components of the device, the drop generator was mounted in a 1 inch outer diameter acetyl cylinder. This cylinder was then secured with a c-clamp to a large acetyl v-block.

4.2 FLUID PROPERTIES

To conduct the intended experiments, it was necessary to use an ink that had a high electrical conductivity for charging and a large enough particle concentration to create a visible mark at deposition. Initially, a sample of black dye-based ink, used commercially in continuous-ink-jet printers was selected. This ink solution was model number L-219, provided by Matthews International Corporation. After repeated attempts at ejecting droplets of this fluid with the Microfab DOD printer, it was found that the high particle concentration of this ink was

unsuitable for use in the system. The concentration was then reduced, by adding solvent, until a working solution was found. The properties of the commercial fluid and those of the resulting solution used in the experiments are given in Table 1 on page 35.

Table 1: Properties of the commercial and experimental inks.

Ink Type	Commercial Solution (L-219)	Experimental Solution (L-219-4:1)
Solvent Base	Methyl Ethyl Ketone	Methyl Ethyl Ketone
Density (kg/m ³)	867	820
Percent Solids	7.1	1.8
Viscosity (cps)	4.31	4.23
Surface Tension(dynes/cm ²)	24.6	24.6
Conductivity (mhos)	1.512E-3	5.46E-4

4.3 SUBSTRATE AND POSITIONING

Because glass is an inert, nonporous material and is well suited for imaging, this was the chosen substrate for deposition experiments. The substrate motion and position were controlled with a two-axis Aerotech xy-linear stage. This positioning table was composed of two ALS20045 linear motors driven with a PC and DR600 amplifier. The Aerotech stage, with the substrate and mounting fixture, is shown in Figure 4.3.1. This motion system provided a positioning resolution of $\pm 1\mu\text{m}$, with a maximum travel speed of 2m/s and a total travel of 0.45m.

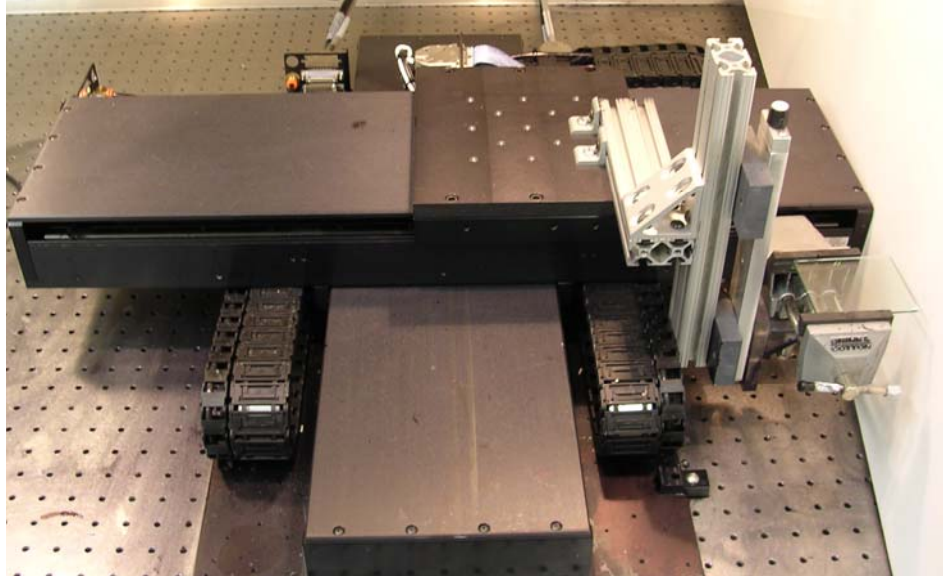


Figure 4.3.1: Aerotech 2-dimensional xy-stage.

4.4 CHARGING MECHANISM

In order to charge the ejected droplets by way of fluid jet polarization, an electric field was created across the point of droplet breakup. This was accomplished with the installation of two charging rings surrounding the ejector tip. The two annular electrodes, machined in type 303 stainless-steel, had an outer diameter of 0.25 inches and inner diameter of 0.0625 inches. These electrodes were also imbedded in an acetyl cylinder of 1 inch outer diameter for mounting. The charge tunnel is shown in Figure 4.4.1, below, and is included in the schematic of Figure 4.5.1.



Figure 4.4.1: Image of the droplet charging mechanism.

The voltage potential applied across the charge tunnel electrodes was generated with a variable DC power supply and an Emco High Voltage F10 DC/DC converter. This setup created a variable voltage from 0 to 1000VDC.

4.5 DEFLECTION

In order to define the operating conditions for the focusing device, it was necessary to determine a relationship between the amount of voltage applied to the charge-tunnel electrodes and the resulting electric charge on the droplets. As shown by Halyo et al, observation of the motion of microdroplets in electric fields is a practical method for extracting the value of charge residing on them [3], [12]. Toward this end, the charged droplets were ejected into a constant, high potential electric field applied in the direction normal to their velocity. From their consequent motion in the field, the magnitude of contained electric charge for the droplets was found. The setup used for these measurements is shown in Figure 4.5.1. The capacitor plates were machined in type 303 stainless-steel and were mounted on a 1-inch diameter acetyl cylinder at a distance of 8mm apart. A potential of 1000V was applied to the deflecting plates, creating a field-strength of 8N/C.

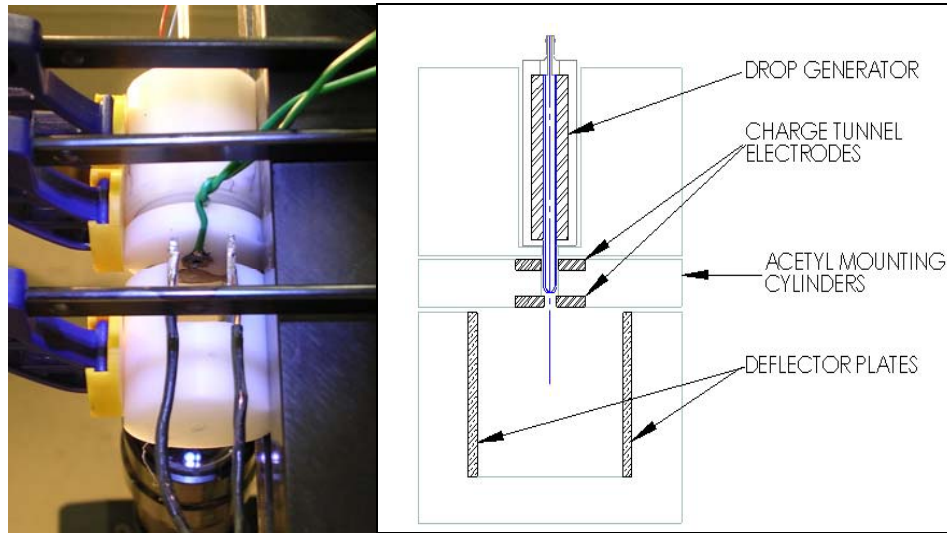


Figure 4.5.1: Image and schematic of droplet charging and measurement setup.

4.6 IMAGING SYSTEM

In order to monitor droplet formation and perform measurements of position and velocity, a Sencam High Speed CCD camera with SVGA resolution was used. This camera allowed the capturing of images with exposure and delay times as small as $1\mu\text{s}$ and as large as 10ms. An Infinity KC lens assembly was used in several configurations providing different magnifications. The frame sizes used in the experiments were $W_{IF4}=2\text{mm}$ and $W_{IF3}=1\text{cm}$, generated with the Infinity F4 lens at a depth of field of 2.5 inches and the Infinity F3 lens at a depth of field of 12 inches, respectively. The camera, shown in Figure 4.6.1, was mounted on a 2-dimensional xz-stage made from 8020[®] aluminum extrusion and friction bearings with attached Velmex linear slides for precise control of positioning.

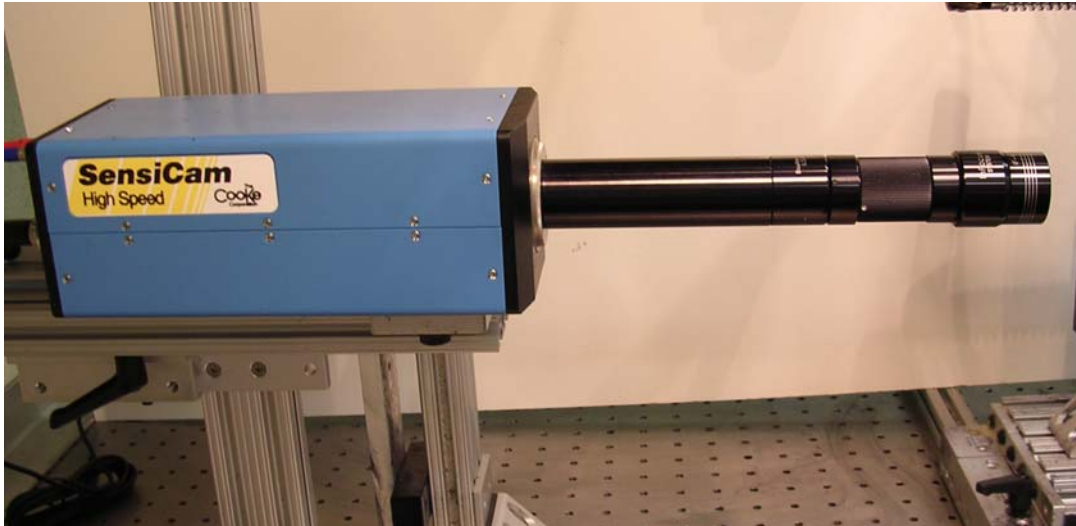


Figure 4.6.1: Image of the CCD camera and mounting system.

The images were triggered using the rising edge signal for drop generation from the analog output card. Because the camera software permitted a maximum delay of 9ms before image capture, a Dynascan 3300 pulse generator was used to provide extended delays for downstream images.

An array of ultra-bright light-emitting diodes was used to provide the backlight illumination for the pictures. The luminous intensity of the LED's, adjustable from 500 to 5000 mcd, was controlled with a variable voltage DC power supply. The positioning of this light source was achieved with a Velmex 2-dimensional yz-stage.

4.7 THE QUADRUPOLE DEVICE

In commercial quadrupole devices, round rods, which closely approximate the correct hyperbolic electrodes, are used. This modification is made to avoid the excessive manufacturing costs for the ideal geometry. It has been shown, however, that the resulting faults in the electric field, caused by the misshaped electrodes, can be minimized by using a radial spacing according to the relation

$$r_0 = r/1.148,$$

where r_0 is the field radius and r is the radius of the electrodes [1]. Since precision shafts are only commercially available in certain sizes, the electrodes for the quadrupole were machined from precision ground, type 303 stainless-steel rods, 0.125 inches in diameter. From the above relation, the rods were mounted at a center-to-center spacing of 0.331 inches. To provide axial alignment with the charge tunnel and drop generator, the mounting fixtures were 1 inch outer diameter acetyl cylinders.

The length of the electrodes chosen for these experiments was 3.00 inches. This length was dependent on many of the other system properties. To prevent small air currents from disturbing the motion of the droplets, a polycarbonate casing was machined to enclose the device. An image of the quadrupole device with attached charge tunnel is shown in Figure 4.7.1, below.



Figure 4.7.1: Image of the linear quadrupole device.

The voltage signals necessary for the operation of this device were generated with an HP33120A function generator and Trek PZD700 amplifier. An image and schematic of the complete setup used for the quadrupole focusing tests are given in Figure 4.7.2 and Figure 4.7.3, respectively.

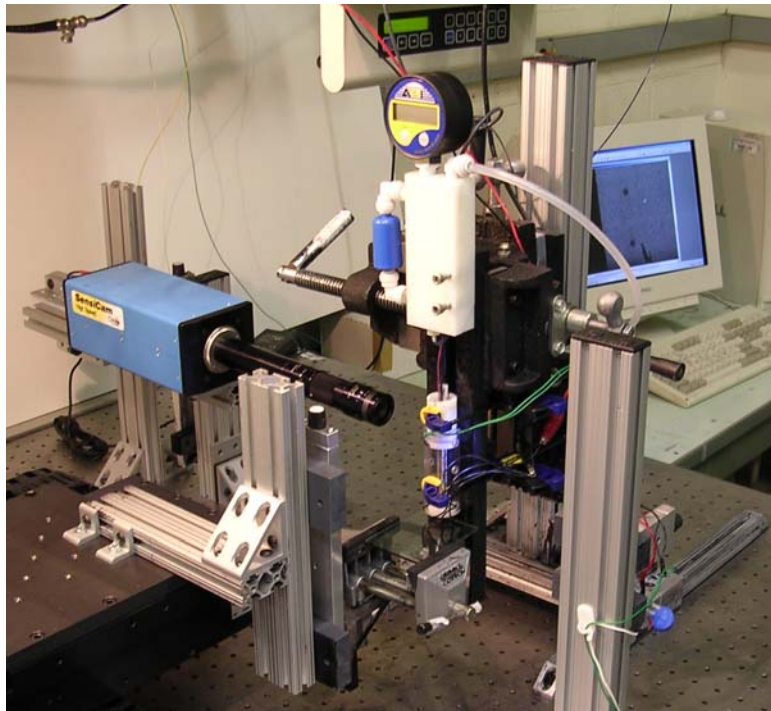


Figure 4.7.2: An image of the testing system for quadrupole focusing experiments.

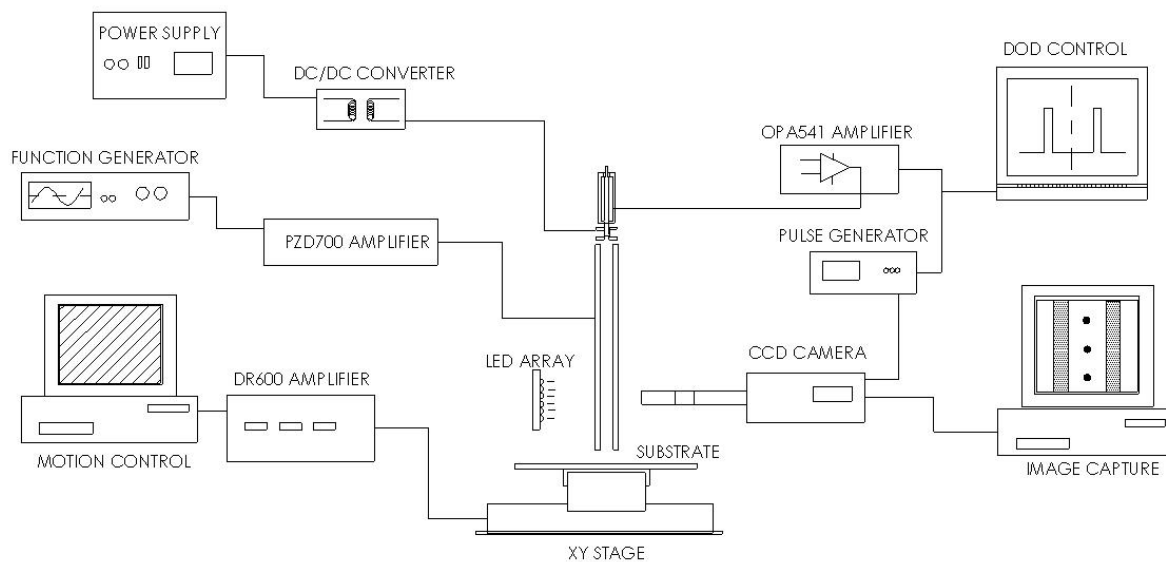


Figure 4.7.3: Signals and Controls for quadrupole focusing experiments.

5.0 EXPERIMENTS AND RESULTS

5.1 DROPLET EJECTION

As illustrated in Sections 2 and 3, the focusing capabilities of the linear quadrupole are dependent on many of the other system variables. So, before performing experiments with the device, it was necessary to find the attainable ranges for these variables. The first step in defining a set of working parameters for the system was to determine conditions for consistent and reliable drop generation. The voltage signal which was sent to the piezoelectric element in the print head, defined the compressive force on the glass pipette and thus the characteristics of the flow out of the orifice. Using the CCD camera to monitor droplet formation, the frequency, amplitude, and duration of the driving voltage were adjusted until consistent results were obtained. As mentioned previously, the region into which the droplets were ejected was enclosed by a polycarbonate shield to reduce disturbances from small air currents. Image 1 of Figure 5.1.1 shows the effect of overdriving the drop generator with a high-frequency signal. This picture was generated with four $15\mu\text{s}$ exposures taken at $100\mu\text{s}$ delays. The drop generator was driven at 500 Hz with a $125\mu\text{s}$ voltage pulse of 28V. The resulting flow was a misdirected spray of random droplets.

By reducing the frequency, the flow was stabilized and the droplets became consistent for each pulse. Drop formation for the same amplitude and duration signal used in Image 1 of Figure 5.1.1, but at a lower frequency of 100Hz, is shown in Image 2. Although the flow in this situation was fairly stable, the observed satellite droplets made these conditions unacceptable for use in the focusing device. By making fine adjustments in the pulse amplitude and duration, the formation of the satellites was impeded. Image 3 of Figure 5.1.1, generated with six $15\mu\text{s}$ exposures at $115\mu\text{s}$ intervals, shows the ejection of

a singular droplet, for a voltage pulse of approximately 27V amplitude and 122 μ s duration at a frequency of 100Hz. This is the drive signal that was used for the remainder of the experiments.

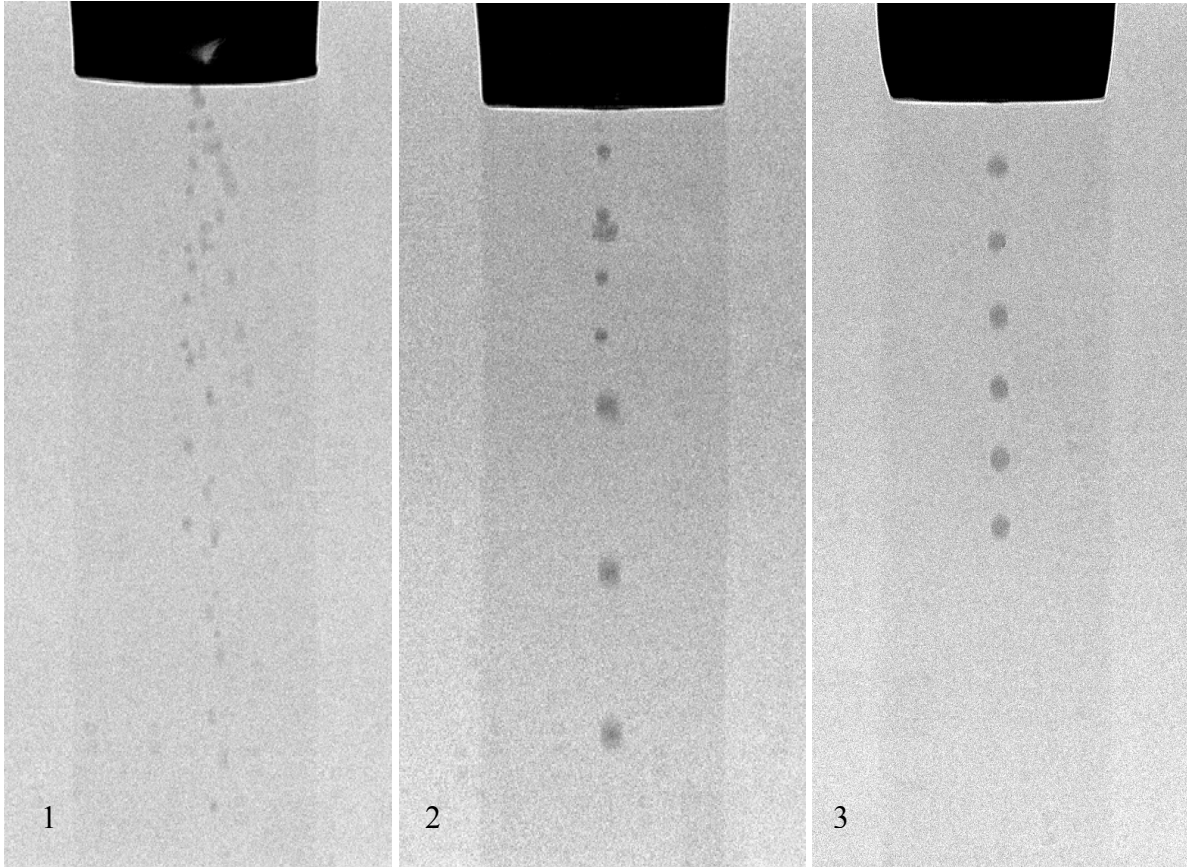


Figure 5.1.1: Images of (1) unstable ejection, (2) satellites, (3) single droplet.

After defining conditions for stable droplet generation, measurements of initial diameter and velocity were taken. In the images, the outer diameter of the glass nozzle was used as a length scale for the calculations. For the voltage signal of 27V and 122 μ s, the resulting ejected droplets had a measured diameter of $62 \pm 2.5 \mu\text{m}$ and initial velocity of $2.1 \pm 0.05 \text{m/s}$. The bias errors listed for these calculations resulted from the finite resolution of the images. Using the IF4 lens, the pixel size for the images was approximately 2.5 μ m. By fixing the time between exposures and

increasing the initial delay before image capture, downstream measurements of the velocity were taken. Several images, taken at different distances from the orifice, are shown in Figure 5.1.2, below.

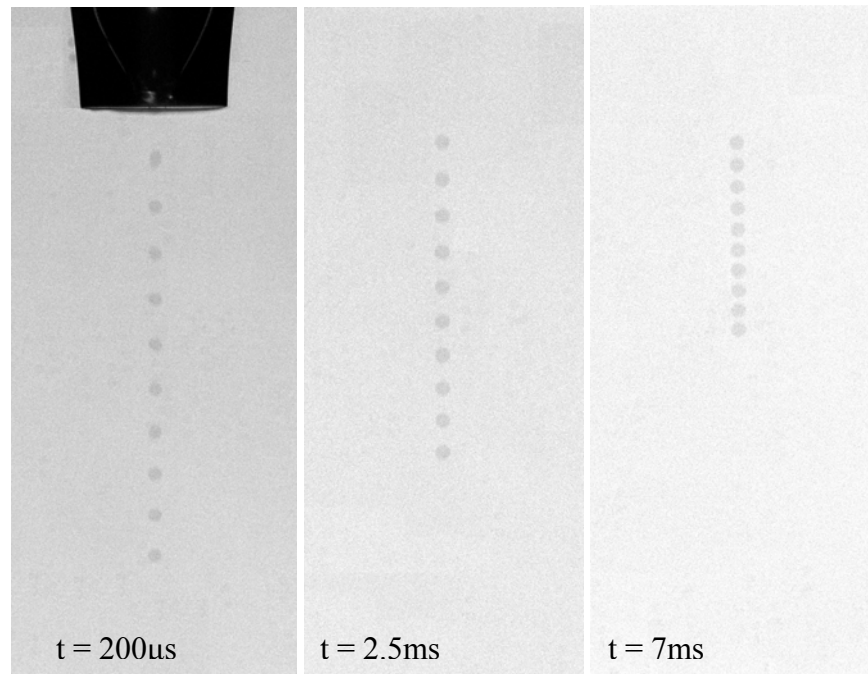


Figure 5.1.2: Images of velocity progression for ejected microdrops.

These pictures were taken with ten $15\mu\text{s}$ exposures at $100\mu\text{s}$ delays. The times displayed on the images of Figure 5.1.2, are the delays for the first exposure, measured from the rising edge signal for drop generation. Calculations of velocity were made in this way for times up to 15ms. The irregularities in trajectory from the drop generator prevented measurement at points further downstream. The calculated velocities from these images are shown in Figure 5.1.3, below.

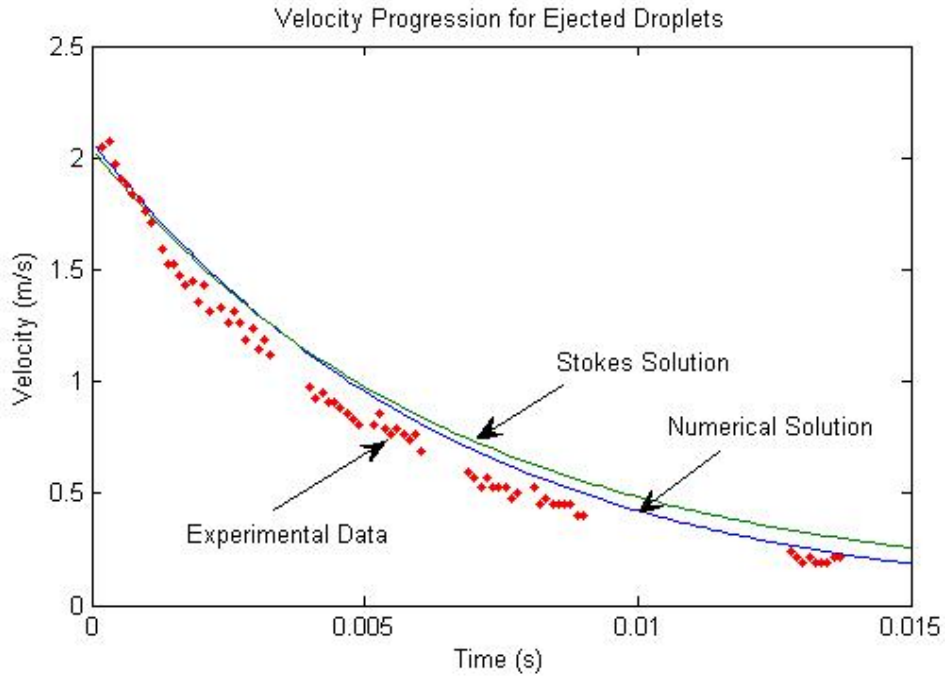


Figure 5.1.3: Plot of experimental and numerical data.

Also plotted in Figure 5.1.3, are the velocity profiles obtained with the theoretical Stoke's solution and the numerical calculations. As expected, during the relaxation period, the numerical solution with Oseen's value for the viscous drag force appears to provide the best fit for the data. However, both solutions are within the range of uncertainty for the measurements.

5.2 CHARGING AND DEFLECTION

Another variable necessary for defining the trajectories within the device was the magnitude of charge residing on the droplets. As described in Section 4.3, this value was controlled with the voltage applied to the charge tunnel electrodes. In order to find the relationship between these variables, the droplets were ejected into an electric field between two parallel capacitor plates.

The displacements of the droplets in the direction of the field were recorded with the CCD camera. In Figure 5.2.1, below, the droplet trajectories for several different charge tunnel voltages are shown.

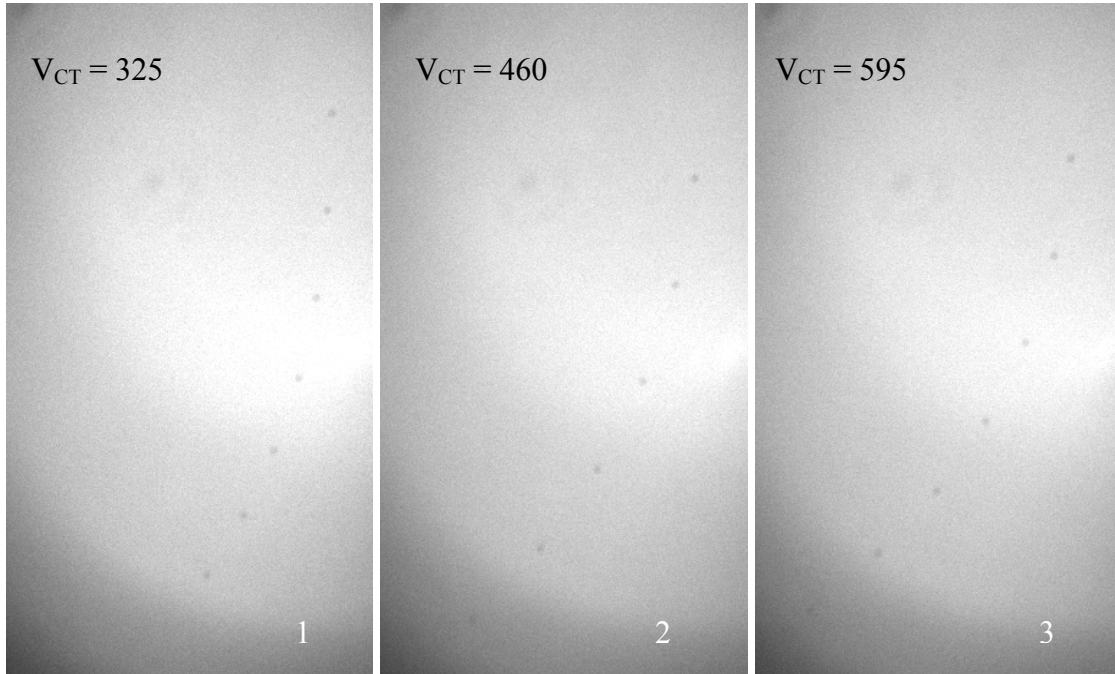


Figure 5.2.1: Images of droplet motion in a uniform electric field.

The voltage was applied to the charge tunnel by connecting the lower electrode to the positive potential and the upper electrode to ground. In this way, the droplets contained a net negative charge. In the figure, the electric field of the deflector plates is acting in the horizontal direction, from left to right. Assuming that the field is uniform and using the data from these images, the acceleration and corresponding magnitude of charge were determined with Equation 2.1.2. As can be seen in the plot of Figure 5.2.2, these calculations yielded an approximately linear relationship between the voltage applied to the electrodes and the induced charge.

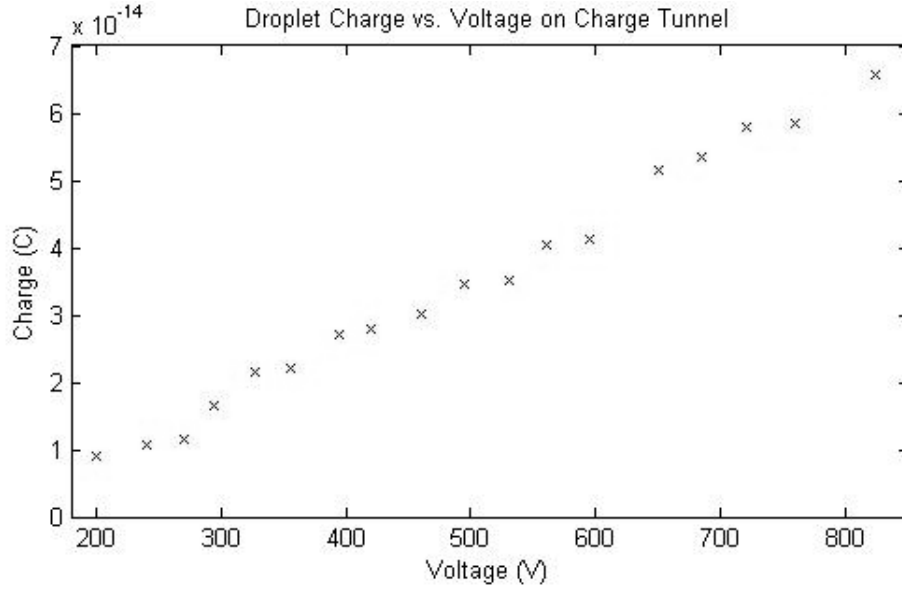


Figure 5.2.2: A plot of the calculated droplet charge according to the voltage applied to the charge tunnel electrodes.

5.3 QUADRUPOLE FOCUSING

The nature of particle motion within the quadrupole device is defined by the values of the coefficients q and K , as well as the off-axial initial conditions. These coefficients are defined by

$$q = \frac{2eV}{m\omega^2 r_0^2} = \frac{6eV}{4\pi\rho a^3 \omega^2 r_0^2} \text{ and } K = \frac{6\pi\mu R}{m\omega}.$$

The initial radius and the magnitude of contained electric charge for the droplets were determined in the experiments of Section 5.1 and 5.2, respectively. The radius of the quadrupole, r_o , was defined by manufacturing considerations (see Section 4.6), and the zero-to-peak amplitude of the applied potential was limited to $V < 700V$ by the characteristics of the amplifier used. The initial density of the fluid, given in Table 1, and the viscosity of air were also easily obtained.

At this point, the only undetermined value in the coefficients necessary for defining conditions of stability was the constant β , used in the approximation of the changing droplet radius (Equation 3.2.1). As previously stated, due to the irregularities in trajectory from the drop generator, measurements of the droplet velocities and radii were not practical at large intervals after ejection. So, in order to determine the value of β , the quadrupole device was necessary for reducing the off-axis fluctuations. However, because β defines the change in the stability properties of the droplets with time, it was necessary to estimate this value for the initial experiments.

As shown in the schematic of Figure 5.3.1, the irregularities in trajectory from the drop generator define the off-axis initial conditions for the device. So, from the images used in Section 5.1 for the calculations of vertical velocities, the off-axis displacements and velocities were also found. From these tests, the largest observed angle of ejection was approximately $A = 2$ degrees from the quadrupole axis.

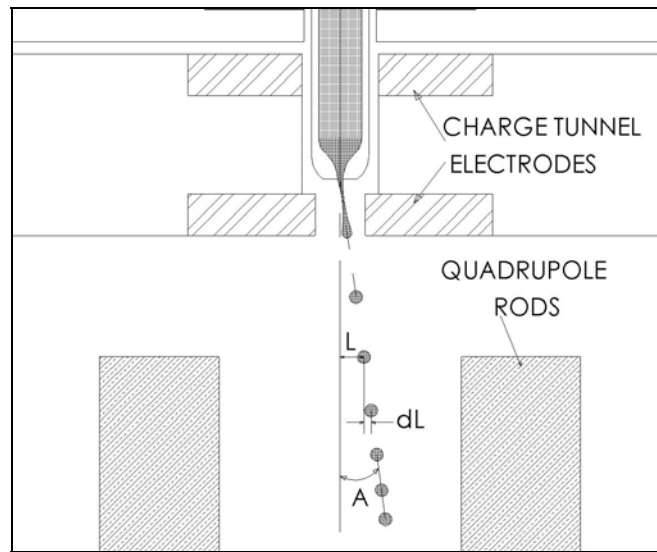


Figure 5.3.1: Geometry of the quadrupole entrance region.

The initial off-axial displacement in the x-direction is defined by the manufacturing accuracy of the mounting fixtures and also by the angle of ejection. The droplet generator is mounted with the tip approximately 4mm from the ends of the quadrupole rods. So, assuming that the manufacturing tolerances for axial alignment were within $\pm .005$ inches, the maximum initial displacement for the 2° angle of ejection was found to be 4×10^{-4} m. From the numerical results for the vertical direction, the velocity at the entry point is 1.45m/s. The corresponding maximum off-axial initial velocity is then .05m/s.

The values of the parameter q increase with time for the falling droplets, according to the value of β , which at this point was undetermined. So, for the initial focusing tests, in order to prevent the onset of instability due to droplet evaporation, a value of q much lower than the stability limit was used. With an applied voltage of 500V zero-to-peak amplitude and frequency of 200Hz, the value $q = 0.2$ was chosen. The plot of Figure 5.3.2, below, was obtained by performing the numerical calculations for the droplet trajectories in the x-direction with the values of the coefficients estimated above. An initial phase of $\phi_0 = \pi/2$, was used in the simulation to provide the maximum expected off-axial displacement.

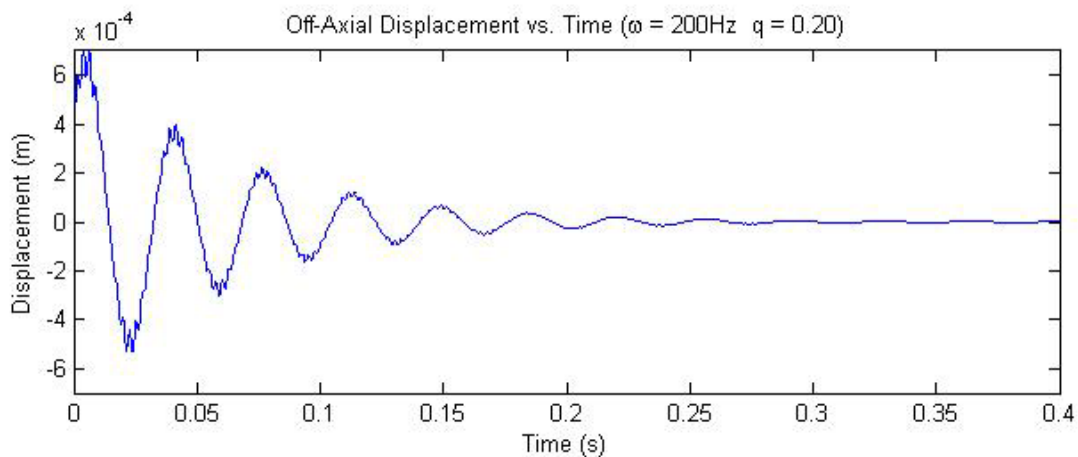


Figure 5.3.2: Numerical simulation of droplet trajectories.

The results from the simulation show a maximum off-axial displacement of $7 \times 10^{-4} \text{m}$ experienced by the droplet. This value was within the geometric restrictions defined by the radius of the quadrupole. Performing the experiments with the device, it was found that the quadrupole did produce stable trajectories for these conditions. An image of the droplets entering the device and a downstream image of the stabilized droplets are shown in Figure 5.3.3, below.

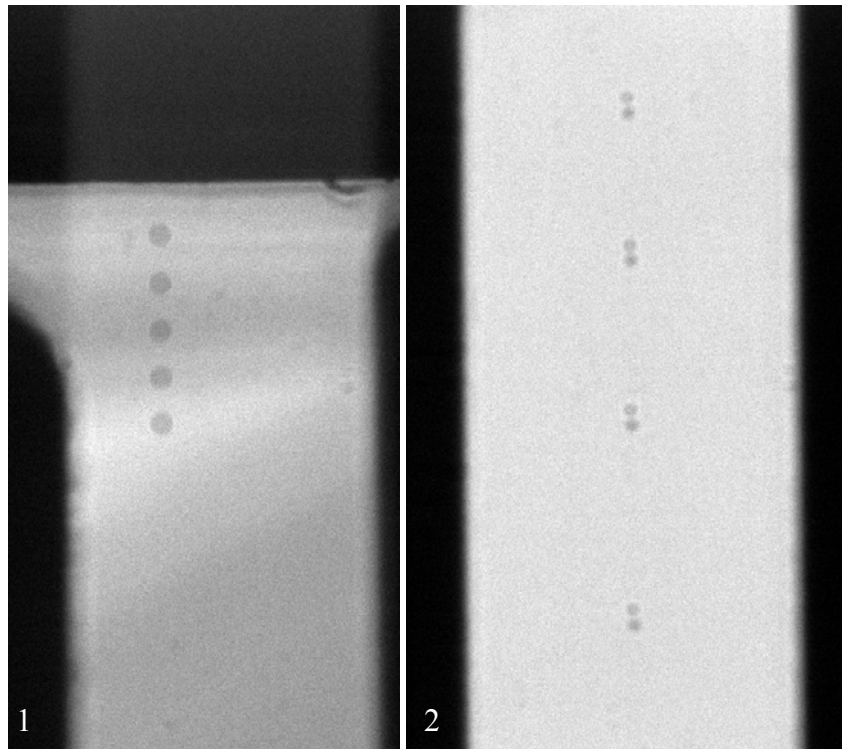


Figure 5.3.3: Images of droplets (1) entering the device (2) 60mm downstream.

The droplets were ejected with a voltage pulse of 27V amplitude and $122 \mu\text{s}$ duration at a frequency of 100Hz. Image 1, in Figure 5.3.3 shows the droplets entering the quadrupole device. The measured initial diameter and velocity at this point were $64 \mu\text{m}$ and 1.4m/s, respectively. The image was taken with five, $10 \mu\text{s}$ exposures at intervals of $100 \mu\text{s}$. Image 2 of Figure 5.3.3,

was taken at a distance of 60mm from the point of entry. This picture was generated with two 50 μ s exposures with a delay of 1ms between them. At this point in the flow, the diameter was found to be $d = 43 \mu\text{m}$, within an error of $\pm 2\mu\text{m}$, and the velocity was calculated as $w = .05\text{m/s}$, within an error of $\pm .01\text{m/s}$. This velocity compares well with the theoretical terminal velocity for a 43 μm diameter droplet of $w_t = .048\text{m/s}$ (Equation 2.2.3).

Using the information of velocity and diameter obtained from these experiments in the numerical calculations for the vertical direction, the time of flight (over 60mm) and value of β were determined to be $\Delta t = .672$ seconds and $\beta = 6.2 \times 10^{-10}$, respectively. Also, because the length of the quadrupole was 76.2 mm, the corresponding time of flight for the droplets from entrance to exit of the device was found to be $\Delta t_e = 1.1$ seconds. For this time period, the diameter of the droplets at the exit point, was found to be approximately $d_f \approx 30\mu\text{m}$.

In Equation 2.2.1, the Rayleigh limit for the amount of electric charge that a fluid droplet can hold is given in terms of the fissility ratio, X . Using a charge tunnel voltage of $V_{CT} = 600\text{V}$ for these experiments, the fissility ratio for the droplets exiting the device was approximately $X = .008$. This value is well below the Rayleigh limit of $X < 1$, so coulomb instability was not a factor under these conditions.

After defining all of the parameters necessary for predicting droplet trajectories, further experiments on the focusing properties of the device were performed. While monitoring the droplet motion with the CCD camera through the viewing window at 60mm downstream, the frequency of the applied potential was adjusted. In the images of Figure 5.3.4, below, the droplet trajectories for different operating conditions are shown.

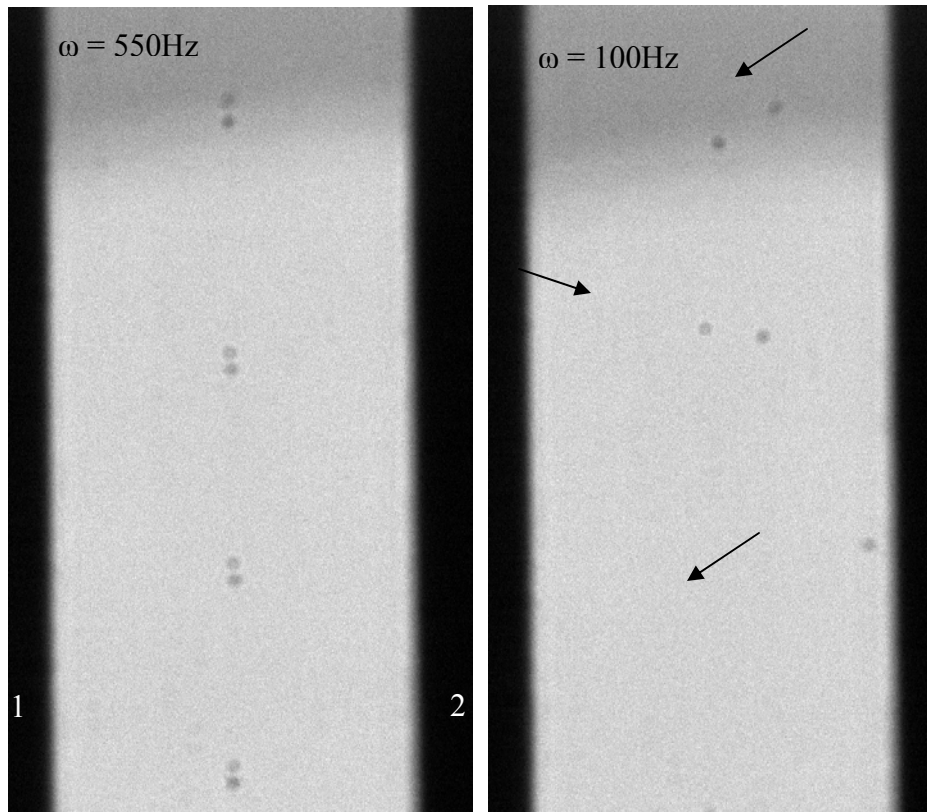


Figure 5.3.4: Images of (1) focused droplets (2) unstable trajectories.

The images in Figure 5.3.4 show droplets created with a drive pulse to the drop generator of 27V amplitude and 122 μ s duration at a frequency of 100Hz. The charge tunnel voltage was 600V and the images were captured with two 50 μ s exposures at a delay of 1ms. For the applied potential in these experiments, an amplitude of 500V zero-to-peak and initial frequency of 1000Hz were used. These conditions, defining a value of $q = 0.005$ at the entrance to the device, did not produce consistent results. The droplet motions viewed in the images were constrained near the central axis; however, their appearance was random. The frequency of the driving voltage was then decreased until consistent, uniform trajectories were observed. This occurred when a frequency of approximately 550Hz was reached, as shown in Image 1 of Figure 5.3.4. After this, the frequency of the applied potential was again decreased until the motion became unstable. Oscillating trajectories, as shown in Image 2 of Figure 5.3.4, were observed when frequency of

approximately 100Hz was reached. Thus, for the prescribed conditions, upper and lower operating limits on the frequency of the applied potential were found to be 550Hz and 100Hz, respectively.

The inconsistent results observed for frequencies above 550Hz can be attributed to the off-axial initial conditions. As described in Section 3.1, for a lower value of the parameter q , the quadrupole field exerts a smaller restoring force, and is, therefore, less able to counteract the off-axial momentum of the droplets. Figure 5.3.5, below, shows the results of a numerical calculation of the maximum amplitudes of oscillation predicted for a droplet traveling through the device. These calculations were performed using the measured values of the necessary variables and the maximum expected initial conditions.

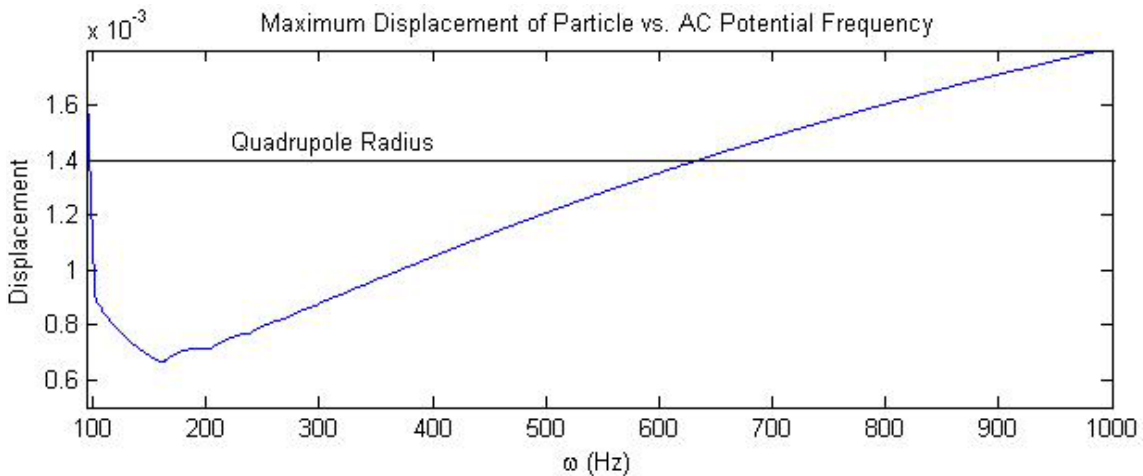


Figure 5.3.5: Numerical results of maximum displacements for experimental conditions.

As can be seen in the plot, the limit of the driving frequency from the numerical calculations was found to be approximately 630Hz. In the simulations, at frequencies above this limit, the displacements of the droplets from the z-axis exceeded the quadrupole radius. Therefore, the numerical calculations predict a slightly higher upper limit for the frequency of the driving

voltage than what was observed in the experiments. The discrepancy in these values is reasonably small and can be easily attributed to the errors in the measurements of the system variables.

From the experiments, the lower limit on the frequency of the applied potential agrees well with the results of the numerical calculations. This instability is caused by the evaporation of the droplets during their time of flight. When a potential with frequency of 100Hz was applied, the droplets, generated with the conditions described above, entered the device with a q value of approximately 0.85. Then, as the radius and mass decreased during flight, the stability limit of $q = 0.91$ was reached, and the droplets began to oscillate with exponentially increasing amplitudes. This explains the motion observed in Image 2 of Figure 5.3.4.

5.4 DEPOSITION

Because the intended applications of this study are in the field of material deposition, it was important to observe the characteristics of the device in this area. In particular, it was necessary to determine whether the droplets, upon leaving the device, could be applied to a substrate. For these experiments, a glass substrate, positioned with the motion system described in Section 4.3, was used. A voltage of 600V was applied to the charge tunnel, and the same conditions for drop generation used in previous experiments were employed. The quadrupole device was driven with a voltage signal of 500V zero-to-peak amplitude and 120Hz frequency, defining value of $q = 0.55$ at the entrance to the device and a value of $q = 0.62$ at the exit. These parameters were selected to provide a large focusing force to reduce the off-axial initial conditions while remaining well within the stability boundaries to allow for some error in the calculations. From the initial results of these experiments, it was found that the stability of the system was very susceptible to mechanical vibrations. In particular, vibrations due to the discrete steps of the linear stage caused inconsistencies in the droplets. The samples printed under these conditions showed random fluctuations in drop placement. By isolating the mounting system for the drop generator and quadrupole, the errors caused by these disturbances were reduced. Another source

of inconsistency was the open geometry of the device at the point of exit. Upon leaving the quadrupole field, the droplets were subject to small air currents and other sources of random motion. These effects were minimized by extending the polycarbonate shield as close as possible to the surface of the substrate.

Although the system did not produce stable and consistent prints for every trial, it was possible to produce several uniform sample traces. Figure 5.4.1, below, shows a comparison of the properties of the resulting marks produced with quadrupole focusing and with standard DOD. A section of 250 μm wire was placed in the frame of this picture for use as a length scale.

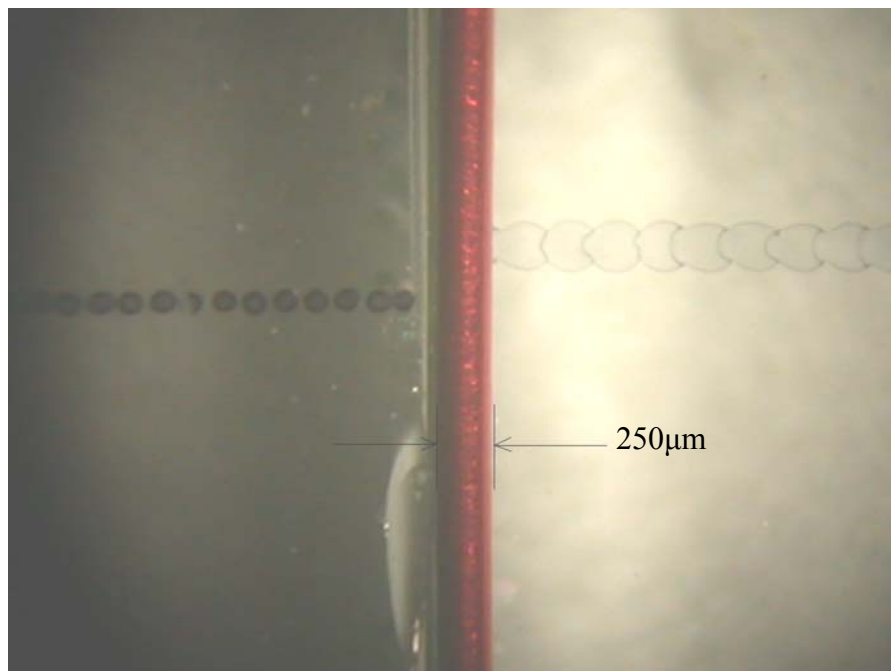


Figure 5.4.1: Marks created with standard DOD and with quadrupole focusing.

The trace on the right side of the image in Figure 5.4.1, was produced by running the piezoelectric drop generator at a frequency of 100Hz with a pulse of 27V amplitude and 122 μs

duration. The droplets were deposited directly on the glass with a distance from the nozzle tip to the substrate of 3mm. The marks on the left in the image were created with the same conditions for drop generation, but by focusing the droplets through the linear quadrupole. It can be seen that the deposition with the quadrupole device created a mark of higher density and smaller width than that produced with standard DOD. The spots produced with the standard method were approximately 240 μ m, while those deposited after traveling through the device were approximately 100 μ m in diameter.

6.0 SUMMARY AND CONCLUSIONS

The purpose of this research was to explore the possibility of using a linear electrodynamic quadrupole to focus microdroplet streams for deposition. The equations of motion for a droplet within the device were derived and integrated numerically. From these numerical calculations, a characterization of the operating conditions of the device was formed, and the effects of the respective constants were considered. An experimental system was constructed, consisting of a droplet generator, charging mechanism, deflector plates for measurement of applied charge, and a linear quadrupole. The attainable ranges of the necessary parameters for this system, such as droplet charge, velocity, diameter, and evaporation rate were found. Experiments with the quadrupole device were then performed to determine the system variables defining the regions of focusing stability. The resulting values were then compared with those of the numerical calculations and theoretical predictions. After this, the device was used in deposition experiments with the stable operating conditions defined in the prior tests.

From the theory of mass spectrometry, it was found that the stability of a charged particle in an oscillating quadrupole field is defined by the parameter q , where

$$q = \frac{2eV}{m\omega^2 r_0^2}.$$

For an AC potential V , of frequency ω , applied across adjacent electrodes, the theoretical stability region is all values of $q < 0.91$. However, the initial velocity and position of the droplets entering the device also affect their motion in the field. In particular, the displacement and velocity in the off-axial directions define the amplitudes of oscillation for the droplets. When q is within the stability bounds, the effect of the periodic quadrupole field is to apply a net force over each oscillation, restoring the particle to the central axis of the device. This net restoring force is dependent on the parameter q and reaches a maximum at approximately $q =$

0.70. Thus, for a given set of initial conditions, a minimum, peak amplitude of oscillation will occur when the system is operated with a value of the parameter $q = 0.70$. For decreasing values of q , the magnitude of the restoring force also decreases. Therefore, when droplets are injected into the device with a large off-axial initial velocity, the radius of the quadrupole defines the maximum allowable displacement and thus the minimum value for the parameter q . The time taken to confine the droplet motion to within some bounds from the central axis, for a given set of initial conditions, is dependent on the frequency of the applied potential. For a constant value of q , this time generally decreases with increasing values of frequency.

Limitations on several of the variables in the definition of q restrict the capabilities of the device. The amount of charge that a droplet can hold is defined with the Rayleigh limit, by the diameter of the drop and the surface tension of the fluid. The maximum voltage potential and frequency are limited by the characteristics of the driving circuitry. Also, the properties of the employed drop generator limit the diameter, velocity, fluid properties, and consistency in trajectory of the droplets. These properties all act to define the useable conditions for operation of the focusing device.

The diameter of the droplet defines its vertical velocity and also affects its stability characteristics in the field. A smaller diameter causes a lower terminal velocity and thus, a longer travel time through the device. This longer time period provides a better opportunity for the modification of the material properties during flight and allows the quadrupole field to further reduce the amplitudes of off-axial oscillation. Also, a smaller diameter will result in smaller feature dimensions on the substrate after deposition. However, because the droplets are evaporating as they travel, this longer time of flight may act to induce coulomb instability. Also, with a smaller terminal velocity, the droplets are more susceptible to deflections from Brownian motion and small air currents. By increasing the diameter, the momentum of the droplets is increased, and, thus the accelerations from these random disturbances are reduced. However, the time of flight, and, therefore, the focusing capabilities of the device are also reduced. In this way, the characteristics of the drop generator and the operation of the quadrupole device will be defined by the requirements of the application.

If a quadrupole focusing device is to be designed to meet a certain DBM need, the limiting factors in the application must first be determined. Starting with the desired material properties of the feature to be produced, an ink is necessary which will decompose by some means to form this substance. Then, the required droplet size, particle concentration, and other fluid properties at deposition need to be defined. After this, if the ink is found to be incompatible with a traditional DOD system, a fluid must be designed which can be altered in some way to form this desired substance. For example, an ink with a low particle concentration that is easily ejected from a DOD head is reduced to a high concentration suspension by evaporation. After an ink and suitable droplet ejection system are chosen, the necessary properties of the quadrupole device can be determined. The characteristics of the drop generator and charging mechanism with the given ink solution will define the initial conditions at the entrance to the device. Also, the travel time through the device will be defined by the necessary droplet properties at both stages and by the mechanism used to alter these properties. Then, using the relationships described in this study, the focusing time and geometry of the device will be defined by the associated ranges of the initial conditions and variables in the definition of the stability parameter q .

It is evident that there are many interdependent variables defining the performance of the device, and thorough consideration of these values is necessary for reliable operation. The experiments performed in this study show that a linear quadrupole can be used to focus charged microdroplets for deposition and that the associated stability conditions can be accurately predicted from the governing equations. The nature of the system may cause it to be impractical for certain applications; however, the results obtained in this research have shown significant potential for use of the technique in droplet-based-fabrication.

BIBLIOGRAPHY

- [1] Dawson, Peter H.. *Quadrupole Mass Spectrometry and Its Applications*. Elsevier Scientific Publishing Company, 1976.
- [2] Lee, Eric R. *Microdrop Generation*. CRC Press LLC, 2003.
- [3] Davis, E. J. and Schweiger, G. *The Airborne Microparticle*. Springer-Verlag, 2002.
- [4] Rayleigh, L. *Philosophical Magazine*. 14:184-186, 1882
- [5] Happel, J. and Brenner, H. *Low Reynolds Number Hydrodynamics*. Prentice-Hall, 1965.
- [6] Langlois, W. E. *Slow Viscous Flow*. The MacMillan Company, 1964.
- [7] Reist, P.C. *Aerosol Science and Technology*. 2nd Edition. McGraw Hill, 1993
- [8] White, F. A. *Mass Spectrometry in Science and Technology*. John Wiley and Sons, 1968
- [9] McLachlan, N. W. *Theory and Application of Mathieu Functions*. Oxford University Press, 1947
- [10] Whetten. N. R. Macroscopic Particle Motion in Quadrupole Fields. *Journal of Vacuum Science and Technology*. 11(2):515-518, 1974.
- [11] Iwamoto, T. Masayuki, I. Theoretical Study of the Stability Characteristics of a Quadrupole Cell. *Aerosol Science and Technology*. 15:127-134, 1991.
- [12] Halyo, V.Kim, P, Lee E. R. Search for Free Fractional Electric Charge Elementary Particles Using an Automated Millikan Oil Drop Technique. *Physics Review Letters*. 84(12):2576-2579, 2000.